Proposal for an

Intermediate Scintillating Fiber Tracker (IFT)

for Run II:

IFT Hardware

Version 2.2

March 26,1995

S. R. Amendolia, F. Bedeschi, G. Bellettini, V. Cavasinni, G. Chiarelli, B. Denby, V. Flaminio, A. Franceschi, S. Galeotti, G. L. Introzzi, A. Menzione, F. Raffaelli
University of Pisa and INFN

K. Hara, T. Kikuchi, S. Kim, K. Kondo, S. Miyashita, I. Nakano, M. Sano, K. Takikawa, K. Yasuoka
University of Tsukuba

M. Atac, P. Berge, M. Binkley, J. Elias, J. Hylen, J. C. Yun
Fermilab

C. Bromberg, J. Huston, R. Miller
Michigan State University

F. Abe, M. Mishina, Y. Morita
KEK

D. Cauz, G. Pauletta, L. Santi
University of Udine

Dario Bisello, Nicola Bacchetta
University of Padova

T. Okusawa, T. Yoshida
Osaka City University

Abstract

We propose a scintillating fiber tracking detector for the high luminosity conditions of Collider Run II where the performance of the inner layers of the central tracking chamber (CTC) will be compromised by high occupancies. The fiber tracker would be located in the intermediate radial space that is presently occupied by the vertex time projection (VTX) detectors. The proposed detector consists of six axial and six stereo cylindrical layers of scintillating fibers, where a layer is constructed as a half-cell staggered doublet of 500 micron diameter fibers. Six layers of axial doublets will provide excellent intermediate R-ϕ track segments that connect the track segments of the SVX II with those of the CTC unambiguously. Due to the fine granularity and hence low occupancy, such system can be fully efficient at very high luminosity. This will complement the inner superlayers of CTC which may be futher degraded by the high occupancy. The axial layers will also participate in triggering, providing precise track segments for use in Level 1 track finding and in Level 2 displaced vertex identification. The six additional doublet layers with stereo angle will each provide unambiguous space point because they are laid on top of the axial layers directly without radial distances, taking advantage of the extremely small fiber diameter. Such superlaye combination of the axial and stereo layers result in excellent 3D pattern recognition of the tracks in high multipicity environment, and can point back to the SVX II with fine Z-resolution. The fiber tracker will cover $|\eta| \leq 1.8$, backing up the four layers of SVX II, so that the central region is completely covered.

The technology and knowledge we have today are sufficient to build such a system. However once the project is approved we would like to carry out an intensive R & D towards further optimization and for detailed design throughout 1995. Further simulation will be made to optimize the layer configuration for the maximum tracking efficiency. We also have a good hope for reducing the material thickness and the cost.

A year and half starting from the beginning of 1996 should be adequate for the construction of the system and one year from mid 1997 will be devoted for the installation and debugging to be ready for Run II that is scheduled to start late 1998 to early 1999.

1. Introduction

The Tevatron has an exciting prospect of very high luminosity after the main injector is completed, up to a few times 10^{32} $cm^{-2}sec^{-1}$ or even higher, at $\sqrt{s}$ of 2 TeV . It enables us to explore the high energy frontier at least for the next decade. It is especially promising after the evidence for top quark production was seen by CDF and D0. In addition we have already proven the CDF's capability of studying B-physics. A robust tracking system operating at a few x10^{32} $cm^{-2}sec^{-1}$ can possibly lead to probing into CP violation in CKM matrix elements.

Therefore it is the time to examine seriously the CDF's capability of maximal use of the luminosity that will be delivered by the Tevatron starting from Run II currently scheduled in late 1998 or early 1999.

One of the main concerns is the tracking system, which has been the most crucial element in the successful physics outcome of CDF. Due to the large drift distance in the CTC, up to ~4 cm, confusion of tracks has already been showing up in the inner super-layers even in the last run. In the future 36 x 36 bunch operation (bunch to bunch interval = 396 ns) and eventual 96 x 96 bunch operation (interval = 132 ns) of the Tevatron, the situation will further deteriorate not only due to the pile up of successive bunch crossings, but also due to the expected high luminosity by increased average number of interactions per bunch crossing up to 2.6. **Fig. 1** shows the average number of interactions per bunch crossing for various operating modes of the Collider.

The outer layers of the CTC will be functional for the immediate future and the new SVX II will provide excellent tracking at small radii immediately outside the beam pipe. Therefore it is imperative to improve tracking in the intermediate region with a detector that will connect the fine tracking by SVX II at small radii to the overall tracking by the outer layers of CTC.

An excellent candidate for such role is a scintillating fiber tracking system of fine granularity.

We propose to install a set of cylindrical scintillating fiber layers in the space between the outer envelope of SVX II and the inner tube of CTC ($r \approx 16.5 \sim 27.7$ cm) that is currently occupied by the VTX. The side view of the proposed scintillating fiber layers in the tracking volume is shown in **Fig. 2.** The basic element is a doublet layer of 0.5 mm OD scintillating fibers spaced by 0.6 mm and staggered layer to layer by a half spacing as illustrated in **Fig. 3.** Due to the staggering, the average thickness is 0.65 mm and virtually there is no inefficiency at the edge of the round fibers. 0.5 mm scintillating fiber with its

effective cell size of 0.3 mm will provide an R-ϕ resolution of the order of 100 μm which is a natural choice for the space between 50 μm silicon strips of SVX II and CTC, where the resolution is on the order of 200 μm per wire. 0.5 mm fibers are also necessary to avoid confusion in the pattern recognition in the high luminosity environment due to extremely high occupancy in this radial range. The estimated resolution of 90 μm for a single staggered doublet layer of 0.6 mm pitch comes as a result of a quadratic addition of the intrinsic resolution of ~87 μm (=0.3 mm/$\sqrt{12}$) and an alignment uncertainty conservatively taken as 25 μm.

A set of six axial layers will provide a stand-alone track segment with a redundancy of three hits. The system is perfectly cylindrical and seamless in azimuth. Preliminary simulation results indicate that four hit points are quite powerful in reconstructing the entangled tracks.

The proposed intermediate tracking layers also provide a track segment in R-Z. both for connecting the R-Z track segments measured by the SVX and the CTC and also to point back the SVX's 90° strips, possibly with its own small angle stereo strips, to find the corresponding track in R-Z view to help disentangle narrowly concentrated tracks. We propose to implement six doublet layers with $\pm\alpha°$ with respect to the beam axis, which is yet to be determined by a detailed simulation. Such superlayers of the axial and stereo fiber combination provide unambiguous space points because the stereo and the axil fibers are essentially at the same radius and the ghost probability is small due to the fine granularity.

Since the fibers are flexible, the stereo layer fibers can be helical and the choice of stereo angle is not limited by mechanical considerations. The limit comes from two factors: the Z-resolution improves rapidly with increasing the stereo angle up to ~10° (See **Fig. 4.**) but flattens out beyond, and the probability of finding ghosts increases almost linearly with the stereo angle (See **Fig. 5.**). If three layers are equally implemented with a combination of U- and V-layers of $\pm$ 3° ($\pm$ 6°) , the Z-resolution is 2.1 mm (0.98 mm) when extrapolated to SVX outermost layer.

It should be pointed out that the configuration of the scintillating fiber layers is flexible because the radial thickness of each super layer is only a few mm and can be adjusted without compromising the performance much once the space required by the SVX II is finalized.

The idea of using scintillating fibers for tracking system is not new. However the following three prong advances in technology have made it a perfectly practical technique. Those are: a) the significant maturity of the solid state photon detector, VLPC, b) the recent

breakthrough in the commercially available fibers, and c) the development of the technology of fiber preparation through the CDF's endplug calorimeter upgrade project.

Because of these new technical circumstances, a scintillating fiber tracking system using 0.5 mm scintillating fibers will be highly efficient, both in individual layer detection efficiency for minimum ionizing particles and in the reconstruction efficiency with excellent pattern recognition capability. It should be reminded that scintillating fiber system is quite similar to SVX because it is more or less a discrete counting device. Other possible wire-based drift chamber type devices would need knowledge of the timing in addition to the registration of the wire positions.

Also the electronics is outside the detector structure and there is no need of mounting massive electronics boards at the end of the sensitive length. The only material in front of the endplug calorimeter face are the clear readout fibers. Plastic connectors for coupling the scintillating fibers to the readout clear fibers add a small mass of low atomic number material at the end of the active scinttilating fibers.

Finally we would like to point out that the scintillating fiber tracking system does not need high voltage or electrically active components within the tracking volume. Therefore, once installed and tested, primarily for the optical connections, the fiber tracker has no need for service accesses into the central tracking volume unless damaged by unexpected cause.

2. Recent Development in Technology

2.1 VLPC

Since the initial test[1] that proved that VLPC was an excellent low level photon detector with high quantum efficiency (≤80%), built-in high gain (~10^5), high dynamic range (≥10^3), and very low noise (≤2 photo electrons) (See the spectrum measured on the fourth generation prototype, HISTE-IV in **Fig. 6**[2]), there have been several small scale tests[3] by various groups to prove the basic idea of using VLPC as the photon detector.

Simultaneously the conversion of the original military version SSPM to commercial version HISTE has steadily progressed at Rockwell, the company which is the sole holder of the proprietary patent of VLPC. The quantum efficiencies of the HISTE-I through IV are compared with that of SSPM in **Fig. 7**. The conversion was to suppress the infra-red sensitivity of SSPM and increase the quantum efficiency in the blue region.

Recently D0 group[2] has made a successful operation of a 3,000-channel cosmic ray test stand using HISTE-IV. It demonstrated a large scale application of the scintillating fiber-VLPC system was quite manageable. Their result showed that the VLPC can be stably operated in He atmosphere of ~6.5° and the number of photoelectrons and the noise level for such large scale operation is essentially the same as what was observed by previous small scale tests by other people. It also demonstrated that the quantum efficiency of the HISTE-IV was ≥70 % to be compared to the ideal quantum efficiency of ~85% of SSPM. **Figs. 8a** and **8b** are the dependence of the quantum efficiency and the rate of the noise (≥1 p.e.) of SSPM and HISTE-V, respectively, on the operating voltage.

These facts eliminate some of the original negative perceptions against VLPC. There was a legitimate concern on the completion of the R&D by Rockwell that it might be terminated at an arbitrary moment. The HISTE-V chips have been produced recently and the preliminary results of the evaluation show that the quantum efficiency is on the order of 70% and the noise level is as good as SSPM as originally hoped for. Furthermore Rockwell now sees market of VLPC in medical and other applications besides the high energy physics. Therefore, although there could still be a valid concern on the reliability of Rockwell as the sole supplier, in regard to the pricing and the delivery schedule, the very basic doubt on the wisdom of relying on the VLPC as the only adequate photon detector has been already crossed out.

2.2 Fiber Development

A major breakthrough was made on the plastic optical fiber technology at about the time when CDF started the endplug calorimeter upgrade project. Kuraray, one of the companies specialized in the plastic optical fibers and scintillators, found a technique to apply another low refractive index cladding over the ordinary PMMA cladding. After initial trials, now it is well established and all the fibers we use in the ongoing endplug upgrade are such "multiclad" fibers to be distinguished from ordinary "single-clad" fibers. **Fig. 9** illustrates the structure of the multiclad and single clad fibers.

The material for the outer cladding is fluorinated-PMMA with n=1.42 which is not new. It has been used as the cladding for PMMA core (n=1.49) plastic fibers for short distance optical connections for computers. Though it is obvious that a cladding with such lower refractive index will yield a larger light trapping aperture because of larger total internal reflection angle, it was materialized only after a technique was developed to use PMMA as an inner cladding because the fluorinated-PMMA does not adhere well directly to the core material, polystyrene (n=1.59). It still have achieve the same total internal reflection angle because according to Snell's law of refraction, the total internal reflection is determined by the smallest reflactive index, 1.42 of the outer cladding in this case, among multiple layers of different indices. Only slight sacrifice is made because the intermediate layer takes, though small, finite thickness, 6% of OD, out of the diameter of the fiber otherwise could be used as the core.

With

$$n_{core} = 1.59 \text{ and } n_{outer\ clad} = 1.42,$$

the total reflection angle within the core, measured with respect to the fiber axis, is

$$\theta^{multi}_{total} = \cos^{-1}\left(\frac{1.42}{1.59}\right) = 26.74°$$

to be compared with

$$\theta^{single}_{total} = \cos^{-1}\left(\frac{1.49}{1.59}\right) = 20.43°$$

for single clad fiber.

This in turn makes the solid angle in one direction

$$\Omega^{multi} = \frac{1}{2}\left\{1 - \cos\left(\frac{n_{clad}}{n_{core}}\right)\right\}$$

$$= \frac{1}{2}\left\{1 - \frac{1.42}{1.59}\right\}$$

$$= 5.35\ \%$$

to be compared with

$$\Omega^{\text{single}} = \frac{1}{2}\{1 - \frac{1.49}{1.59}\}$$
$$= 3.14\ \%.$$

Therefore the "aperture" of the multiclad fiber is 60% larger after taking account of the 6% smaller core diameter compared to a single-clad fiber of the same diameter. In order to use small diameter fibers necessitated for better resolution and low occupancy, this is an important advantage. **Fig. 10** is an illustration of such relationship.

2.3 Tools and Techniques for Fiber Preparation

The endplug calorimeter upgrade project[4] is in the last phase of the production of the scintillator tile/fiber panels. Panels for E.M. section have been all made and the production of the hadronic section is going to be finished by the end of the year.

This upgrade project is the first large scale use of optical plastic fibers for a real calorimeter and is significantly different from other type of fiber-based detectors because individual fiber is a link of a chain that determines the calorimeter uniformity in a few to several % level. Therefore they were prepared with a highly systematic way and the necessary tools and techniques were developed prior to the mass production. At every step, the qualities of the fibers were quantitatively monitored.

First of all, we have obtained a set of statistically significant data on the commercial fibers and found that they were very much satisfactory in terms of tolerances in various parameters.

The tools we developed include single-fiber finishing diamond machine, connector finishing diamond machine, and fusion splicing machine. They have been heavily used throughout the production process and the results have been remarkably consistent. The mirroring of the fiber end is not what we have developed but our massive use proved the quality of aluminum sputtering for mirroring simultaneously proving the quality of the fiber finishing.

We have been monitoring the quality of the commercial fibers carefully because it is the basis of whole technology. We now know that the uniformity of the roundness and the diameter are excellent. **Fig. 11** is a microscope photograph of a cross section of a scintillating fiber cut by the diamond fly-cutting machine and **Figs. 12a** and **b** are the histograms of the measured diameter sampled over 16 km and 20 km of the fibers, respectively. Further detailed data taken online in the process of drawing 0.9 mm OD clear fibers were submitted by KURARAY. The diameter was mesured at every cm over the delivered 50 km and the result were a) mean value = 0.90135 mm with b) R.M.S. =

0.591 % after rejecting c) 238 points that exceeded 40 μm limit. The histograms for every 2.2 km were all well symmetric around mean value with well behaving tail. The mean values of those 25 histograms (one histogram was missing.) ranged between 0.8966 and 0.9092 mm. From such data, we can safely specify the diameter tolerance of ±2 % as the real maximum.

The light output and the attenuation length, which are dependent on the purity and the concentration of the fluor and the mechanical uniformity of the core-cladding structure, has also been very consistent. **Fig. 13** is a histogram of the light output from fibers sampled over the entire period the production of E.M. tile/fiber panels. A ~70 cm long fiber was sampled at every 150 meter waveshifter fiber over the total of 16 km and inserted into a piece of scintillator tile. Using a Sr^{90} source shining the tile, the light output from 30 cm pigtail was mesured by a photototutbe. The R.M.S. variation is 2.9 % for 116 entries. Obviously the result is a combined effect of the diamter tolerance and the fluor concentration uniformity.

Fig. 14 is a histogram of the reflectivity[4] of the mirrors made by aluminum-sputtering on the end of waveshifetr fibers. The measurement was made by directly comparing the light output before and after the mirroring. Therefore the quality of the fiber end finishing together with the mirroring should be the main factor with small measurement accuracy. The entries with 0.8 or lower in the reflectivity are due to faulty operation of the aluminum sputtering machine at one time due to contamination by other metal.

Most of these tools and techniques are what we need to use for the fiber tracking and the endplug calorimeter upgrade project has been an immensely valuable experience on how to handle fine fibers for optical system and how to monitor them.

As a conclusion of this chapter, we find that scintillating fiber tracking is a viable solution for the tracking in the intermediate radial region where fine granularity is essential. Fine granularity directly means a sizable number of channels, but we have the technique and experience to handle such large numbers of fine optical fibers.

3. Conceptual Configuration

3.1 Overall Design

Since the design of the SVX II has not been finalized, we take the non-"Draconian" 4-layer design* and the CTC's inner tube as the "default" boundary condition.

*It is not difficult to accommodate the 6-layer design as currently presented without changing the performance of the scintillating fiber tracking we propose.

The 4-layer design calls for the leg of the "positioner" at 165 mm as the largest radius and the CTC's inner tube ID is 277 mm. Therefore we assume that the proposed intermediate fiber tracking occupies the radial range between 165 mm and 270 mm. The sensitive length in Z-direction is 1.6 meter as the default design whcih may be extended to 2.2 meter if the simulation results allow larger occupancy without sacrificing the reconstruction efficiency.

As the default design until the configuration is optimized by a detailed simulation, there will be six super layers built on a composite materail cylinder and each layer is separated by 18 mm. Therefore the radii of those layers are at r=180, 198, 216, 234, 252, and 270 mm. The composition of these layers is : (U, V, Z), (Z), (Z), (U, V, Z), (Z), (U, V, Z). The sketch of the r-ϕ profile is shown in **Figs.15a.**

There are three concentric cylinders each carrying an odd nubered super layer and a successive even numbered super layer. In each cylinder, the odd numbered super layers is on the inner suface of ~18 mm thick RHACELL core and the even numbered layer is on the outer surface of it., each epoxied over a carbon fiber cloth. The procedure of assemblying such structure is to start with the innermost carbonfiber cloth spread over a collapsable mandrel and the structural layeres are built over it one by one. The carbon fiber cloth will provide a strength along the plane of the memblane and the ROHACELL core will provide the thickness perpendicular to the memblane to provide the strength against the bending moment. Excellent long term stability is expected due to near zero value of the thermal expansion coefficient of the carbon fiber.

44 μm thick carbon fiber cloth woven out of 7 μm fibers is commercially available and it should makes a strong composite structure with ROHACELL # 31, with perforation to remove 2/3 of the material. The perforation will not have much effect on the strength because of the strength of the carbon fibers in the membrane. The subsequent layers are built identically increasing the radius by 18 mm each

time. Thus we will have three independent shells which are supported at the both ends. If necessary it is imaginable to have a low mass ring which supports and adjusts the mid point.

As shown in **Fig.15b**, in those layers that consist of axial, Z-, and stereo, U- and V-, layers, the fiber layers are laid directly over the others and epoxied. The stereo layers are with $+\alpha°$ and $-\alpha°$ with respect to the Z-axis.

Each of the fiber layers is a staggered "doublet" layer of 0.5 mm^{OD} scintillating fibers spaced at 0.6 mm center to center as shown in **Fig. 3**. The effective sensitive cell is therefore about 0.3 mm considering the core of the fiber to be 0.44 mm. Therefore the expected resolution is ~0.3 mm/$\sqrt{12}$ = 0.87 μm. If we assume a tolerance of ~25 μm which is a conservative estimate including all the effect, especially the tolerance of the fiber diameter, 2% of the OD or 10 μm as the maximum, and the positioning accuracy of 25 μm** or better, the overall resolution is estimated to be 90 μm.

** Fiber positioning of D0 group's exercise. After the fiber position is measured as a gentle function of the position in Z and corrected in the software by parametrization, the residue was ~10 μm.

The material thickness is tabulated in **Table 1**. The total weight is about 14 kg per meter in the length evenly distributed along the axis and in azimuth..

The structural strength is being studied by finite element analysis, and, though preliminary, it has been shown that such structure is highly rigid. If the cylinder is supported at the both ends, naturally the sag is the largest at the midpoint along the axis. The entire cross section of the cylinder saggs by 50 μm without deforming the circular shape. Therefore the structure is very strong and the sag is almost negligible, or could be easily corrected with a small numbre of parameters. In this calculation the length of the cylinder was 2.2 meter and was supported at the both ends assuming a flange inserted into the structure at each end. The result for 3.1 meter is in the same range.

In the above analysis the fibers are taken as a simple load. Although a super layer consists of an axial fiber doublet layer and one or two stereo doublet layers with certain angles epoxied together make a complete cage, most of the strength is from the carbon fiber cloth.

A separate study was made in which a cylinder was assumed to be made by only a single layer of 64 μm carbon fiber cloth and optical fiber layers, U, V, and Z, all epoxied together. Even such a structure turned out to be strong enough and the maximum sag at the midpoint was 20 μm. Therefore the above result is

convincing. Test is being carried out to find out the strength with realistic arrangement of 0.5 mm fibers.

Furthermore, it seems possible that the entire structure is laid in the carbon fiber plastic tube of the CTC's inner wall. The load to the wall is calculated to be be ~1/2 or smaller of the total weight, ~42 kg provided the cylinder is supported at the place of the CTC's endplates. Such scheme might be needed if the SVX II needs to be supported by the intermediate scintillating fiber tracker. Such scenario will be studied futher. A mechanism for precise alignment is also under study.

The advantage of such design of three independent shells each carrying two super layers is that all fiber layers are accessible after they are completed either by a radioactive source or by a UV or X-ray source directly. Therefore the calibration of each fibers to find out whether there is any damage is trivial. Futhermore, using proper collimator and or trigger counter of fine resolution, possibly another set of scintillating fibers or silicon strips, it is possible to survey all the fiber positones as constructed. Then after three shells are assembled into a single structure, the overall alignment can be made with cosmic rays before seeing real events in the collision hall. Naturally real events will be used at least for the confirmation of the alignment over entire azimuthal angles.

I is also possible to imagine an in situ calibration/monitoring moving a light source or radiaoactive source in the gaps between the shells.

Table 1. Material Thickness

Radii mm	Thickness mm	Material	Density	X_0 (Comment)	Rad L
First Layer	(Average thickness of fiber doublet $=\frac{\pi}{4}$ x 0.5 mm x 2 x $\frac{1}{1.2}$ + 0.1 mm (Epoxy) = 0.7545 mm)				
179.5	0.044	Carbon Fiber Cloth (44 μm)	2.265 g/cm^3	18.8 cm (Solid Graphite)	0.0234
179.5	0.1	Epoxy	1.16~1.2 g/cm3	34.4 cm (Plexiglass)	0.0291
179.5~180.5	1	Fiber Doublet (Z)	1.032 g/cm3	42.4 cm (Polystyrene)	0.1779
	0.1	Epoxy			0.0291
180.5~181.5	1	Fiber Doublet (V)			0.1779
	0.1	Epoxy			0.0291
181.5~182.5	1	Fiber Doublet (U)			0.1779
Sub Total	3.0				0.6444 %
Spacer					
182.5	0.1	Epoxy			0.0291
182.5~197.5	15	ROHACELL #31	1/3 x 31 mg/cm3	40.55 g/cm^2	0.0382
197.5	0.1	Epoxy			0.0291
	0.044	Carbon Fiber Cloth			0.0234
Sub Total	15				0.1198 %
2nd Layer					
197.5	0.1	Epoxy			0.0291
197.5~198.5	1	Fiber Doublet (Z)			0.1779
Sub Total	1				0.2070 %
3rd Layer					
215.5	0.044	Carbon Fiber Cloth			0.0234
215.5	0.1	Epoxy			0.0291
215.5~216.5	1	Fiber Doublet (Z)			0.1779
Sub Total	1				0.2304 %
Spacer					
216.5	0.1	Epoxy			0.0291
216.5~233.5	17	ROHACELL #31	1/3 x 31 mg/cm3		0.0433
233.5	0.1	Epoxy			0.0291
	0.044	Carbon Fiber Cloth			0.0234
Sub Total	17				0.1249 %

4th Layer						
233.5	0.1	Epoxy				0.0291
233.5~234.5	1	Fiber Doublet (Z)	1.032 g/cm3	42.4 cm	(Polystyrene)	0.1779
	0.1	Epoxy				0.0291
234.5~235.5	1	Fiber Doublet (V)				0.1779
	0.1	Epoxy				0.0291
235.5~236.5	1	Fiber Doublet (U)				0.1779
Sub Total	3.0					0.6210 %
5th Layer						
251.5	0.044	Carbon Fiber Cloth				0.0234
251.5	0.1	Epoxy				0.0291
251.5~252.5	1	Fiber Doublet (Z)				0.1779
Sub Total	1					0.2304 %
Spacer						
252.5	0.1	Epoxy				0.0291
252.5~269.5	17	ROHACELL #31	1/3 x 31 mg/cm3			0.0433
269.5	0.1	Epoxy				0.0291
	0.044	Carbon Fiber Cloth				0.0234
Sub Total	17					0.1249 %
6th Layer						
269.5	0.1	Epoxy				0.0291
269.5~270.5	1	Fiber Doublet (Z)	1.032 g/cm3	42.4 cm	(Polystyrene)	0.1779
	0.1	Epoxy				0.0291
270.5~271.5	1	Fiber Doublet (V)				0.1779
	0.1	Epoxy				0.0291
271.5~272.5	1	Fiber Doublet (U)				0.1779
Sub Total	3.0					0.6210 %
Light Shield						
	0.04	Tedler Film	1.39 g/cm3	28.7 cm	(Mylar)	0.0139
TOTAL	**107.5**					**2.9 % X_0**

WEGHT/SHELL : 3.6~5.0 kg/meter : Fibers : 0.203g / m x (15,616~ 21,760) = 3.2~4.4 kg/m,
: ROHACELL : 2π (18~27)cmx1mx17mmx1/3x31mg/cm^3 = .2~.3kg/m
: Carbon Fiber : 2π x 2(18~27)cm x.044 mmx2.265g/cm^{3}x1m = .2~.3kg

The numbers of fibers are shown in **Table 2** for the assumed radii. Total of ~57,000 fibers is necessary for such configuration.

Table 2. Number of Fibers

(Default Configuration)

Radii	Views	Circumference	No. of Fibers /Doublet layer	No.of Views
180 mm	U, V, Z	1,130.97 mm	3,770/View	x 3
198 mm	Z	1,244.07 mm	4,147/View	
216 mm	Z	1,357.16 mm	4,524/View	
234 mm	U, V, Z	1,470.27 mm	4,901/View	x 3
252 mm	Z	1,583.36 mm	5,278/View	
270 mm	U, V, Z	1,696.46 mm	5,655/View	x 3
Total				**56,927 Fibers**

The scintillating fibers are each mirrored at one end and the other end is connected to a 5 meter long, 0.8 mm diameter clear fiber. The sizable step in diameter of the clear fibers was necessary considering the tolerance of the alignment of the fibers at the junction and the better transmission for the larger diameter fibers through 5 meter path length to the VLPC.

The connection is made by optical connector which is a simple extrapolation of the 10-fiber connectors developed for endplug upgrade project although the number of fibers will be 128 per connector. Based on our experience, the alignment tolerance is in the range of 10 μm. The junction between the connectors is filled with a 25 μm thick film of soft RTV for index matching that eliminate Fresnel reflection which other wise cost 10 % in the light transmission through air gap.

Light shielding is provided by black Tedlar film covering the inside and the outside of the entire stack. The film continues to cover the clear fibers routed through "30° crack between the endplug structure and the central structure to the end of the clear fiber bundles at the entrance into the cryostat to be mounted on the rear face of the endwall. The space at the end of the cylinder needed for such connections expected to be within the space curren ly used by CTC, namely 5 cm for the endplate, and 10 cm for the high voltage and preamp boards in Z-direction*.

*The test made for the endplug upgrade project has consistently proved that the bending 0.83 mm fibers does not affect the light transmission even in long term if the radius is larger than 2 cm.

4. Optical Readout by VLPC

4.1 VLPC

The photon detector is VLPC which is an acronym of silicon device, Visible Light Photon Counter. A microscope photograph is shown in **Fig. 16**. The characteristic of VLPC is summarized in **Table 3**.

The HISTE-V produced recently is 70 ~ 75 % in quantum efficiency according to the preliminary evaluation and it is expected to achieve ~80 % close to the military version SSPM's QE of 85 %.

The noise level has been shown to be ≤1 photoelectron. The gain was ~20,000 for HISTE-IV and became 80,000 for HISTE-V with the operating DC voltage of 6.5 V. The linearity and the repetition rate is only dependent on the areal saturation by the number density of photons each creating an avalanche of about 10 μm in lateral profile. Though the area within such an avalanche is saturated for ~10 μ sec, the accidental overlap of two photons hitting the same spot within the cell, 1 mm round for our choice, is extremely small** especially for the fiber tracking in which average number of photons is expected to be ~10 per MIP.

**A test showed no saturation up to 3,000 photons into one cell.

The rise and fall time is faster than a few ns. Therefore the output pulse shape is dominated by the amplifier's rise time and the decay time of the scintillator fluor of ~10 ns in exponential decay time constant.

The operating point has to be ~6°~7° K which can be provided by holding the VLPC in a He gas atmosphere slightly above liquid He level. It has been demonstrated that maintaining the temperature within ±0.5°*** for stable operation is not difficult with a simple temperature monitor and a resistor as a heater.

*** If cooled lower than 6°, the quantum efficiency drops and at temperature higher than 7° the noise level increases though the quantum efficiency does not increase beyond a plateau. See **Fig. 8b**.

4.2 Cassette and Cryostat

Since the VLPC has to be kept in a cryostat, the signal light brought by 5- meter long clear fiber has to be guided into the surface of VLPC by another clear fiber bundle from the top of the cryostat down into the cryostat in an assembly dubbed "cassette". **Fig. 17** is an illustration of the cassette.

Table 3 Characteristics of VLPC

Effective Quantum Efficiency	$\geq 70\%$
Noise of ≥ 1 Photoelectron	≤ 5 k Hz
Average Gain	$\geq 8 \times 10^4$
Gain Dispersion	≤ 30 % for single photoelectron
Dynamic Range	10^3 (Linear)
Pulse Rise Time	≤ 3 ns
After Plulse	none (≤ 0.01 %)
Saturation Pulse Rate	2.5×10^7 Hz
Average Current	(200 + 300 cc.) nA
Average Power	~ 1.3 μW
Operating Voltage	6 ~ 7 V
Breakdown Voltage	7.5 V
Operating Temperature	6° ~ 7 ° K
Dynamic Range	10^3 (Linear)
Magnetic Field Effect	None up to 1.2 Tesla
Neutron Damage Level	$\geq 10^{10}$ n/cm2

The connection of the fiber bundles at the top of the cassette is again made by an optical connector. The clear fiber in the cassette is chosen to be 0.9 mm in diameter that provides a plenty tolerance for connecting with incoming 0.8 mm fiber and allows an unavoidable tolerance for connecting with VLPC.

The clear fiber surface does not touch the VLPC in order to avoid possible damage of the VLPC because of the quite different thermal expansion coefficients**** between plastic and silicon.

****The thermal expansion coefficient of commonly used plastic, including polystyrene, is $20 \times 10^{-6}/°C$ or 1.6 % for 300°C temperature change whereas for silicon it is $3 \times 10^{-6°}/C$ or smaller than 0.1 % for 300°C change.

The jump from 0.9 mm of the fiber diameter to 1 mm diameter sensitive aperture of VLPC allows ~30 μm tolerance in the alignment, which is inclusive of the fiber diameter tolerance of 2 % or 18 μm, the ~20 μm clearance of the hole on the fiber holder at the fiber end facing VLPC, and the relative alignment error between the fiber end holder and the VLPC of ~25 μm, and the gap up to ~75 μm between the end of the fiber and the VLPC surface. It should be reminded that the envelope of the light cone, once exiting from the fiber, becomes

$$\sin^{-1}\left[\, 1.59 \times \sin\left\{ \cos^{-1}\left(\frac{1.42}{1.59}\right)^{*} \right\}\right] = 45.7°. \qquad \left({}^{*}\cos^{-1}\left(\frac{1.42}{1.59}\right) = 26.7° \right)$$

Such arrangement is illustrated in the cartoon in **Fig. 18.** .

Therefore a conservative allowance of the gap between the fiber end and the VLPC, which is not easy to control, necessitates the seemingly large step from the diameter of the fiber to the VLPC sensitive area.

VLPC's are made into 8-cell chips, as shown in **Fig. 19**. The sensitive round window is 1 mm^{D} and the center-to-center spacing is 1.05 mm. Each cell is connected to a square pad for micro-wire bonding. **Fig. 20** is a photograph taken under a microscope with a magnification of 50. Sixteen such 8-cell chips are laid in a row making up 128 channels corresponding to a single cassette that houses 128 channels of incoming fibers. The back of the VLPC chips is soldered onto an aluminum nitride substrate with each of the VLPC cells micro bonded to the printed lines on the substrate. A cable connecting these lines carry the signal through the cassette to the outside of the cryostat where the readout electronics board is mounted. A common DC bias voltage of 6~7 V is supplied to the soldered VLPC backing with respect to the readout pads.

By implementing simple "buffer" with felt around and inside the cassette, the top of the cassette can be at room temperature without dew condensation while the bottom of the cassette, ~20 long, is exposed to the temperature of the VLPC, i.e., 6.5°K.

The aluminum nitride substrate was chosen as a material that has the same thermal expansion coefficient as the VLPC which is a silicon device so that there will be no mechanical stress on the VLPC chips.

The substrate is also expected to provide uniform temperature to the VLPC chips since the VLPC's power consumption is only ≤ 1.5 μ Watt.

The cassette, with the incoming fibers and output cables, naturally brings in heat from the outside. Therefore a careful thermal design has to be incorporated with the cassette design. Based on the successful experience, the substrate will be soldered onto an oxygen-free copper tray and the whole assembly will be housed in a high purity (≥ 99.999 %) aluminum casing which is cooled by penetrating pipes of two-phase liquid He. The pure aluminum casing is to provide well-controlled 4.2°K environment to the copper tray The chamber is also filled with He gas. The substrate is cooled to the desirable operating temperature 6°~7°K by He gas being cooled by the surrounding aluminum casing at 4.2°K. He gas flows upward through the vertical column of the cassette to "pre-cool" the fiber and cable bundles so that the proper temperature gradient between the top of the cassette and the bottom is maintained to minimize the heat flow from the outside.

The necessary operating temperature is maintained to $\pm 5°$ around the required temperature by a sensor-heater pair, each a small resistor, connected to a simple temperature monitor-controller on the outside. However it has been learned that a proper adjustment of the relative position of the copper tray with respect to the aluminum casing and also the adjustment of the gas flow through the cassette at the outlet can bring the temperature close to the desired value without much activating the heater thus minimizing the He consumption.

It has been known from the past tests that the proper operating temperature and the voltage do not vary element to element within the same production batch and the gain variation is within ~10 % with the same operating condition.

We take the design of the substrate developed by D0 as a default design. The design has incorporated what has been learned in the past tests and, in our judgment, it is a well-thought design. Also there is a possibility that Rockwell provides the substrate with all VLPC chip's micro-bonded and tested. It is natural to expect that by combining our order with D0's order, the price will be significantly reduced.

Fig. 21 is a drawing of the cryostat developed by D0 which houses 12 cassettes corresponding to 1536 channels. Again we take this design as the default although there could be some change dependent on detailed assessment of the boundary conditions on how they are mounted at the back of the endwall.

5. Choice of Fibers and Optical Consideration

5.1 Choice of Fibers

In Run II, luminosity of up to ~2 x10^{32} $cm^{-2}sec^{-1}$ is expected. Even if the number of bunches is increased to 96 x 96 with bunch spacing of 132 ns, the average number of the interactions, taking 46 mb as cross section of the "visible" interactions, becomes 2.6 per bunch crossing. Any high PT collision event generates about 3 MIP equivalent number of tracks. 0.5 mm OD fibers are necessary for such condition in order to avoid the confusion in the pattern recognition directly with its small granularity and indirectly by suppressing the occupancy or the ghost probability.

However one has to be sure about the expected number of photoelectrons for MIP.

First, multiclad fiber is definitely favored because of the 60 % larger "aperture" as discussed in earlier chapter, and also superior mechanical properties. Due to the mechanical strength and the flexibility of the outer cladding material, fluorinated polymer, multiclad fibers are much more flexible and durable than single clad fibers whose cladding, PMMA is known to be brittle. Though the multiclad fiber has PMMA as the inner cladding it is secured and well protected by the outer cladding. Possibly due to such mechanical stability which most likely prevent unnoticed micro-cracks of PMMA, the attenuation lengths of the multiclad fibers are consistently better than that of single-clad fibers whose PMMA clad is exposed without protection. **Fig. 22** is a comparison of the attenuation curves of a multiclad fiber and a single clad fiber.

The scintillating fiber will be 1,500 PPM 3HF fiber, with 1% PTP as the primary fluor. 1,500 PPM has been measured[5] to be optimum for the light output for a 1 meter or longer fiber. **Fig. 23** is a test result showing that the peak light output is obtained at ~1,500 PPM for 1 meter, 2 meter and 3 meter points. Once the fiber is longer than ~20 cm there is not much change in the output spectrum due to its large Stokes shift that is the unique feature of 3HF fiber. In case of ordinary scintillation fluors with small Stokes shifts, there is always non-negligible overlap between the absorption spectrum and the emission spectrum. Therefore along the path of the emitted light through the fiber, the shorter wave length end of the emitted light is gradually absorbed by the overlapping long wave length end of the absorption band. This is observed as a fast decay component in the attenuation curve. In contrast, 3HF has uniquely long Stokes shift due to its proton transfer mechanism and there is no overlapping between the absorption band and the emission band. Therefore the observed attenuation curve is well described by a single, long exponent and also the measured spectrum at 20 cm and 3 meter is not much different in

shape, as shown in **Fig. 24**. Also due to the spectrum peaking at green, 530 nm, the attenuation length is uniquely long, 5 meter for 0.83 mm multiclad scintillating fiber and 7 meter in a clear fiber as shown in **Fig. 22**. This also means that it is the strongest fiber found so far being less susceptible to the possible radiation damage[6].

The optimum value for the primary fluor PTP has also determined experimentally to be 1 %.

The rise time of 3HF is about the same as any other scintillating fiber, ≤ a few ns, and the decay time constant is ~12 ns. **Figs. 25a** and **b** show the oscilloscope trace of the signal from 3HF and its integration, respectively.

Long term stability of 3HF has been studied[7] recently. If it is exposed to UV containing light source at an intensity over certain threshold level, there is a noticeable degradation in the, light output. On the other hand there is no permanent damage if the light intensity does not exceed certain limit. The condition for fiber tracking is far below such "threshold" and no damage is expected as long as the material is not exposed to open day light or strong fluorescent lamp.

**Recently two other scintillation fluors have been synthesized and tested in a fiber. The result is similar to that of 3HF. However the concentration is half, for the optimum light output, of that of 3HF for "Vinyl 3HF" and further 1/4 for "FG231". Also "FG231" has a decay constant of ~10 ns and we are still investigating whether this type of fluor can be made into brighter fiber.

5.2 Optical Consideration

Table 4 is a step-by-step account of the number of photoelectrons. The starting point is the number of photons generated by a MIP that is, according to particle booklet, 1 photons/100 eV energy deposit. From various test results, this number well holds, on conservative side, for the number of photons in a 1500 ppm 3 HF (1% PTP) fibers. The light capturing aperture of a multiclad fiber is 5.35 % as discussed in Chapter 2, and taking 0.5 mm OD, the average number of photons to be "captured" is 33.7 for a MIP traversing the fiber perpendicularly at the edge of a 0.3 mm effective cell of the core.

Though the fiber is 1.6 meter long the far end is helped both by the angle of the traversal of the particle and also by the mirror. Therefore the weakest signal is from 90°, or η=0 point. The attenuation length of 0.5 mm 3HF fiber, 3.37 m is an interpolation of the data of 0.7 ~1.0 mm fibers and 60 μm fiber[8].

Table 4 <NUMBER OF PHOTOELECTRONS>

0.5 mm OD (Core = .88 OD = .44 mm),

0.6 mm Spacing Staggered Doublet

Effective Cell =.3 mm, Min Thickness at the Edge=.7315 D_{core}

3HF(1500 ppm, 1% PTP), Double Clad

1 photon /100 eV energy loss

<dE>min = .5 mmx0.88*x.7315** x 1.032 g/cm^3 x 1.9 MeV/(g/cm^3)
*Core OD, **Min thickness
= 63.1 keV
=> 631 photons

Magnetic field effect (+7%) => 675 Photons

Fiber Capturing Efficiency : One direction $\frac{1}{2}(1-\frac{1.42}{1.59}) = 5.346\ \%$

No. of photons : **36.9 Photons**

		Far End	Midpoint
Length of 3HF to spliced point = L		1.6 m	.8 m
$\theta = \tan^{-1}(\frac{R}{L/2})$	:	19.29°	90°
(L = 1.6, R = 0.28 m)		(η=1.77)	(η = 0)
Angle Factor = 1/sin θ	:	3.03	1
Attenuation thru **3HF** = $\exp(-\frac{L}{3.37*})$	:	0.622	0.788
(* Fiber diameter dependence: L = 1.015 exp(2.4 D))			
Mirroring factor = 1+ Reflectance x $\exp\{-\frac{2x(1.6-L)}{3.37*}\}$			
Reflectance = 0.9	:	1.9	1.56
Attenuation thru **5-m 0.8 mm Clear Fiber**	:	$\exp(-\frac{9**}{12}) = 0.472$	
(**3.6 m to exit to the rear end from r = 20 cm at z=0.8 m , 3.3 meter from 9 O'ck point to 12 O'ck point on the endplug surfac along the 30° crack, and 2 meter as the extra routing)			
Transmission thru Connectors	:	$(0.95)^2 = 0.903$	
Transmission from clear fiber to VLPC	:	0.85	
Quantum Efficiency of VLPC	:	70 %	
Overall Attenuation Factor	:	0.908	0.311
<No. of Photoelectrons>	:	**33.5**	**11.5**

Detection Effic./Layer (≥2 pe**): ≥ 99.8 %**
(****Rockwell's spec for D0 : Noise ≥1 pe : 5,000 counts/sec)

Possible Improvement:
(Q.E. = 80 %) : **(38)** **(13)**

The length of the 0.8 mm clear fiber is taken for the worst case in which the fibers exit the "30°" crack at 9 O'ck point and reaches 12 O'ck point where the cryostat will be mounted routed in a circular path along the "30°" crack. A measured attenuation length for 0.83 mm clear fiber is used.

The reflectivity of the mirror is what has been measured in the end plug upgrade project (See **Fig. 14**) and the transmission through the connectors is the conservative side of the measured values. The transmission through the gap between the clear fiber and the VLPC is a value measured on a connector with air gap.

The quantum efficiency of the VLPC is what has been measured for the HISTE-5.It should be reminded that D0 cosmic ray test was made with HISTE IV which is ~62 % in quantume efficiency with the same measurment.

Taking all this effect into account the overall transmission is 0.3 for the 90° point yielding ~11 photoelectrons. This is the average value at the edge of the sensitive cell of the core for the longest possible clear fiber.

Landau fluctuation and Poisson statistics have to be taken into account to evaluate the detection efficiency. Landau distribution as generated by GEANT, as shown in **Fig. 26** for 0.5 mm polystyrene has a steep tail on the lower side and therefore does not make sizable contribution to degrading the signal compared to Poisson fluctuation. After these two effects are convoluted, the single layer efficiency is plotted in **Fig. 27** for various values of the average number of photoelectrons.

The specification for the noise level being discussed with Rockwell for D0's order, based on the data of HISTE-4 and HISTE-5, is that the noise of ≥1 pe must be 5,000 counts/sec or less. Considering that such number is low enough not to disturb the system performance, the threshold can be conservatively taken at ≥2 pe . Therefore the single layer detection efficiency is ≥99.9 %. It should be reminded again that the above estimate is for the edge of the effective 0.3 mm cell and for the longet route for the clear fibers. Therefore the overall efficiency is much higher than this value and therefore we have enough margin for unexpected decrease of the light due to unforeseen cause.

6. Signal Readout and Electronics

With the gain of ≥80,000 and the average number of photoelctrons to be ≥10, SVX II chip will be adequate for the signal readout providing the signal integrated over ~100 ns* and AD conversion.

*Out of 132 ns cycle, ~25 ns is necessary for the preparation.

It should be noted that rad-hardnes is not required, early non-rad-hard version in the chain of evolution of SVX II chips is adequate for the IFT.

In order to get fast signal outputs for low level triggering as discussed in the next chapter, a front end signal splitter/discriminator circuit dubbed "precursor chip" being developedby UC Davis group for D0 is counted on. The circuit splits the signal from VLPC into two ways, one for the input of SVX II chip and the other for discriminator input. A gate of ~30 ns will be applied at the discriminator to eliminate curling low momentum tracks beyond the necessary readout time. The path length-averaged speed of the transmission within the multiclad fiber is 5.6 ns/m which creates maximum of 18 (25) ns time difference between the direct and mirror-reflected signal for the nearest point on the ±0.8 (± 1.1) meter long sincitllating fiber. However the weakest signal is from the midpoint of the fiber whose reflected signal arrives at the near end 11 (15) ns later than the direct signal from the near end. Therefore the gate may be closed before the latest reflected signal from the near end. The effect of the gate width on the triggering efficiency which might be affected by not waiting the tail of the 3HF scintillation signal will be studied in near future.

7. Level 1 and Level 2 Triggers

Application of tracking requirements for trigger decisions at the earliest practical point in the multilevel trigger structure has been a major factor in CDF trigger strategies. The price to pay for delaying track requirements is in purchasing more bandwidth for the subsequent levels and/or imposing large prescale factors and/or raising physics thresholds. Scintillating fiber detection elements are intrinsically prompt and can easily be used at the first level trigger. The information can also be reused at higher levels of the trigger for pattern recognition algorithms such as tagging secondary vertices or finding the softer leg of a J/ψ candidate. Studies of the performance and optimization of utilizing fiber information in the Run II trigger system are just beginning; the following is an overview description of scintillating fiber participation in the first and second level trigger systems from more of a hardware perspective.

7.1 Level 1

It is our view that tracking information will be required for Level 1 decisions because of the physics goals that require low thresholds for leptons and particular processes like a B decaying to two pions. Without another "handle", the beam conditions of Run II may force the thresholds and prescale factors to unacceptably high values to stay within the Level 1 bandwidth limit. For the intermediate fiber tracker, there is a front end electronics prerequisite before the information can be used at Level 1. The front end electronics proposed is the SVX II readout chip which does not produce prompt hit bits for use by a trigger. A signal splitter or pickoff chip is needed in front of the SVX II chip to produce the prompt signals. At present, work is in progress on such a front end chip at U. C. Davis for the D0 fiber tracker trigger system.

Level 1 stiff track information will be generated by the XFT system working on prompt hit bit information from the CTC. Information from the intermediate fiber tracker would be added to the XFT road search in place of superlayer zero. As shown by A. Baumbaugh for the SDC design, processing the hit bits from fiber superlayers and linking between superlayers is a straightforward operation which can be realized using field programmable gate arrays. Track segments binned in transverse momentum and phi would be available in less than 100 nsec after the crossing, and then saved in a pipeline fashion for later inclusion in the XFT track finding process. Finalization of the fiber diameters and

superlayer radii would include the requirement of proper matching to the ϕ-granularity of the XFT system.

Using simple combinatorial logic, signals from the six axial layers of the IFT can be used to provide hits in 720 phi bins at a radius of 22 cm as an additional input to the XFT processor. In addition, a full standalone IFT trigger, which will also give the above mentioned 720 phi bins as a by product, is being studied by the Pisa and Udine groups. The output of the trigger, in addition to the 720 phi hits, will be the number of tracks found in a set of positive and negative Pt bins (number of bins to be determined).

The current plan is to divide the 6 axial layers into 192 identical phi wedges each containing 150 fibers (excluding overlap regions). The actual numbers will depend upon the final choices of superlayer radii, fiber pitch within the ribbons, and the choice of definition of the overlap regions between wedges (e.g., wedge shaped or butterfly shaped regions) and are not yet decided; however, the exact choice will not influence dramatically our conclusions.

Each wedge will be served by 2 standard cell gate array chips which enumerate all possible track combinations of hits in 5 or 6 layers. A simple simulation has shown that the number of patterns to store is well within the capabilities of existing technology for standard cell gate array chips with of the order of 200 pins. As opposed to the D0 design, we prefer standard cell gate arrays to field programmable gate arrays (FPGA) because experience in the Pisa group has shown that the FPGA's have significantly reduced density and require a very large programming effort. In order to accommodate possible misalignments of fibers or routing errors it is planned to have the fiber signals pass through an on-chip multiplexing layer before passing to the standard cell units, which will allow a remapping of the fiber signals afferent to the chip. The addressable multiplexor lines into the chip will thus allow a certain amount of 'programmability' even in this technically 'nonprogrammable' technology.

Because the standard cell approach enumerates all possible coincidences, the momentum resolution obtained should approach that obtainable offline. Studies of resolution, efficiency, and fake trigger rate are still under study. A cost estimate of this solution is given below.

In addition to the gate array solution, we are also investigating a solution using a neural network-like algorithm. This algorithm can be thought of as making use of 'fuzzy' coincidences between 5 or 6 'groups' of fibers in the different layers, instead of between individual fibers. In order to retain some of the information on the relative positions of the individual fibers, each one enters into the coincidence with an analogue weight which is exponential in its distance from the center of the fiber group. The algorithm is described in

more detail in a University of Udine internal note (available from G. Pauletta, U. Udine). Preliminary results indicate that the achievable momentum resolution is nearly on a par with that obtained offline. The advantage of this algorithm is that the total number of coincidences required is reduced by about 3 orders of magnitude as compared to the gate array solution, thus implying a much simpler chip design. Possible disadvantagess are: 1) The analogue weights may prove difficult (or, at least, expensive) to realize in silicon; and 2) The algorithm is more susceptible to problems caused by high occupancy. Studies are currently underway to evaluate the algorithm and its potential advantages and disadvantages. We do not yet have a price estimate for this solution. The preliminary study has some 300 chips with about 150 inputs each; therefore the cost should not be radically different from that of the gate array solution.

For either solution, it is foreseen to route the discriminated VLPC signals on ribbon cables to large multiwire patch panels which re-route the signals into the gate arrays. Whichever solution is finally adopted, it is important to reiterate that the existence of a trigger makes certain restrictions on the geometry of the detector and the readout path. Probably all fiber ribbons will have the same pitch. This puts restrictions on the ratios of the chosen superlayer radii since a fiber pattern periodic in phi is required for the trigger; i.e., it must be possible to divide the detector into *identical* wedges in order to ensure that a single gate array design will be able to serve for all trigger chips. The routing scheme chosen for the signals must then carefully preserve the geometry of the detector: the standard cell coincidences must operate on groups of signals which come from the same phi slice; coincidences may *not* span chip boundaries. As the design of the IFT becomes finalized, it will be important to keep these restrictions in mind in order not to compromise the very important ability of the IFT to participate in the level-1 trigger of CDF.

The estimated cost of the IFT Gate Array Trigger, with 6 axial fiber layers,192 Phi wedges, 150 fibers per wedge, 2 Gate arrays per wedge is:

Gate Array Chips (includes design, development, prototyping, test runs, contingencies)	$120,000
Trigger Cables (128 conductor)	$ 8,000
Multiwire Trigger Patch Panel Boards	$ 35,000
Power supplies for above	$ 12,000
VME Interfaces	$ 15,000
Total	$190,000

7.2 Level 2

In Level 2 trigger processing, the fibers would be treated in the same way as is planned for the SVX II strips. Adding hits from the axial fiber layers improves the pattern recognition, reduces ghosts and helps with the impact parameter resolution function. Basically, the fibers would be included in the Silicon Vertex Trigger (SVT) as if they were somewhat long strips. The ϕ granularity of 0.5 mm fibers at a radius of 25 to 30 cm is comparable to that of 50 μm pitch strips at a radius of 25 to 30 mm. The data source is also the same as for the SVX II, a trigger-friendly version of the SVX chip; no special new hardware is needed. As was the case for Level 1, the final choices for fiber diameters and superlayer radii include a requirement for proper matching to the phi- granularity of the SVT system.

8. Fiber Layer Assembly Procedure

8.1 Fiber Ribbon

The first process for making fiber layers is to make a ribbon of 128 fibers. Fibers are laid down onto a tray with 128 grooves of the cross section shown in **Fig. 28**. After the fibers of the first layer are laid into the grooves, the second layer fibers are laid down keyed between the first layer fibers. Narrow bridges with identical grooves as the base plate are placed at regular intervals on top of the second layer fibers to guarantee the positioning of fibers. After all the fibers are in place, epoxy is applied. The adjacent fibers are touching each other so that the spacing is maintained primarily by the fibers but not by the epoxy.

Connector is mounted on one end and polished with a diamond fly cutter. The other end is also cured with epoxy, fly cut with diamond machine, and mirrored.

Such process will guarantee the regular spacing between the fibers and when it is transferred from the ribbon making jig, the straightness within the fiber plane is not going to be disturbed if the ribbon is transported by a rigid beam using vacuum suction cups which act to the ribbon only vertically.

Such method has already been routinely practiced by Purdue group[9] for D0, though for 0.835 mm fibers, and the result is quite satisfactory although there is a room for improvement in the accuracy of the of the fiber positioning and also the operation can be much simplified by proper jigs.

Currently both at Pisa and Fermilab, grooved plates are made/being made and ribbon making is practiced with 0.5 mm fibers. **Fig. 29** shows the shape of the groove being expored at Fermilab. This has a much deeper grooves which may ease the operation by better securing the fiber in the grooves. The profile of the grooves can be changed by grinding the tool bit to a proper shape and the first try of round grooves yielded deep groove of a round bottom quite precisely fitting round 0.5 mm diameter gauge pin as shown in the photograph shown in **Fig. 30**.

8.2 Final Mounting

The ribbon is then transferred to the cylinder and epoxied. The rotational positioning of the cylinder is well controlled by a stepping motor. Commercially available stepping motor with an accuracy of 10 seconds (0.048 mrad) gives 13 μm resolution for the fiber ribbon for the largest radius, 27 cm. The fiber positions can be inspected prior to applying epoxy by temporarily tacking the ribbon.

The process of laying down stereo layers is not different from the process for straight axial layers except that the fiber ribbon is laid onto the cylinder at an angle and therefore the cylinder needs to be rotated while the fibers are laid down and epoxied over the entire length.

9. Light Pulsing Monitoring System

We propose to monitor the stability of the response on a channel-by-channel basis by periodically exposing the fibers of each IFT layer to an extended pulsed source of ultraviolet (U/V) light. Extended sources will consist of quartz fibers from which cladding will have been partially removed over a length corresponding to the circumference of an IFT layer. The fibers will be fed by a pulsed U/V laser.

It has been verified in the laboratory that an extended source of U/V light can be created in this manner. The cladding was etched away from one side of a 600 micron diameter fiber by means of a sharp pointed instrument over a length of 60 cm (corresponding to the circumference of an IFT layer) near the end of a 30m long quartz fiber which was optically coupled to a pulsed nitrogen laser. It was verified that; (a) the intensity of the light escaping from the damaged fiber was sufficient to excite the scintillating fibers and (b) that the attenuation length, although dereased by partial removal of the fiber cladding, is nevertheless long enough to enable a sufficiently uniform distribution of U/V light over a length corresponding to the circumference of an IFT layer. (Details of the test can be found in a note obtainable from G. Pauletta).

One partially exposed quartz fiber per IFT layer will be introduced into the detector via the 33 degree crack and the partially exposed end of each fiber will be wrapped around an IFT layer and fixed with the exposed side in contact with the layered fibers. The fibers will be pulsed periodically by means of a pulsed U/V laser. Laser pulses will be shorter than the decay time of the fiber scintillator so that the time dependence of the channel response to the U/V stimulus can also be monitored. Laser power will be sufficient to generate more than 10**4 photons per pulse in order to have a better than 1% check of the channel response stability. The laser instability of ~ 3% will be factored out by viewing the end of each fiber with a PIN diode and dividing the laser-generated signals from the VLPC's by the PIN-diode output. It has been verified that one can monitor stability to better than 0.3% by means of this technique.

A similar technique will be used to monitor the upgraded plug calorimeter reponse, and the IFT monitor can be integrated into the plug monitor if the laser power is upgraded from that presently forseen for the plug, thereby saving considerable expense.

The cost of the proposed monitor comes mainly from the cost of upgrading the laser and of acquiring and etching the additional quartz fiber. A breakdown of the estimate is as follows:

laser upgrade	$ 20,000
quartz fiber	$ 14,000
PIN diodes	$ 2,000
other materials	$ 10,000
fiber etching	$ 5,000
machine shop	$ 5,000
tech time	$ 10,000
total	$ 66,000

10. R & D

In order to optimize the system and finalize the design in detail, we need to carry out some R & D in the earliest possible future.

The R & D can be reasonably well phased into the overall schedule taking advantage of the different degree of the needs of the R & D.

The longest time required for the fabrication is for the fiber lay-down process. Fortunately fiber ribbon making is one of the least of the needs for technical exploration and also it is almost independent of the development of the other components. Therefore the ribbon making can be started at an early phase in parallel with the process of finalizing the design of other components.

There are items that appears to need expertise of the outside company. The first of such items is the support cylinder whose good dimensional accuracy with long term stability is the basis of the tracking accuracy. The R & D on such item needs to be started at the earliest possible point.

Most of the works need engineering and a few technicians for prototyping in addition to the financial support.

We are also hoping to carry out a beam test of a prototype segment of about 1500 fibers to find out the real parameters such as R-ϕ and Z resolution, the detection

efficiency,and the effect of δ-rays, simultaneously gaining an experience on such system including the cryogenics and readout electronics.

The following is the list of the components that need R & D. In order to meet the dead line for the installation and debugging in 1997 through 1998, most of the R & D has to be finished by mid 1996.

Table 6 R & D

Items	Comments
Fiber Ribbon Making	Already underway. Minor both in the complexity and in the cost. Due to totally different fiber diameter we have to do the job independent of D0.
Support Cylinder	Major task. The prototype cylinder made by SSC related R&D showed excellent precision and strength but much more than what we need in terms of material thickness. There is a significant room for reducing the material thickness for our application.
Fiber Mounting on the Cylinder	Major task. Needs CORDEX machine long enough to survey 3.1 meter length. Needs early study and practice with ordinary (card board) cylinder.
VLPC substrate	Wait for D0 design to be completed within a few months. Most likely it satisfies our needs. Slightly differnt design is being studied at Pisa.
Cassette	Wait for D0 design to be completed. Most likely the design needs to be modified because of our specific constraint.
Cryostat	First wait for D0 design to be completed. It is possible that we need to modify it significantlly for our specific constraint.
Support structure	Major task. Need engineering for overall structure compatible with/including SVX II.
Readout electronics	Expecting SVX II chips to be completed in time. Expecting input splitter/discriminator chip, "prcursor chip", for fast signals for Level-1 trigger be completed in time for D0.

11. Cost Estimate

Table 8 COST ESTIMATE

Fiber Layers

Radii	Views	Circumference $2\pi R$	No. of Fibers $\frac{2\pi R}{0.6}$ x2		No. of Views		No. of Cassettes per View		(128 chan/cassette) Total
177.23 mm	U, Z	1,113.57 mm	3,712 / View	x	2		29 / View	x 2	= 58
195.57 mm	V, Z	1,228.80 mm	4,096 / View	x	2		32 / View	x 2	64
213.90mm	U, Z	1,343.97 mm	4,480 / View	x	2		35 / View	x 2	70
232.24 mm	V, Z	1,459.21 mm	4,864 / View	x	2		38 / View	x 2	76
250.57 mm	U, Z	1,574.38 mm	5,248 / View	x	2		41 / View	x 2	82
268.91 mm	V, Z	1,689.61 mm	5,632 / View	x	2		44 / View	x 2	88
Total			**56,064 Fibers**						**438 Cassettes**

Labor

	Engineer	Technician
Cassette	1 x 2 months	2 x 12 months
Cryostat	1 x 2	
Cylinder/Fiber Ribbon Mounting	1 x 1	3 x 4
Support structure	1 x 2	2 x 1
Cryogenics/Plumbing	1 x 1	2 x 1
Fiber Ribbon Making		2 x 12
Cable Making		2 x 6
Cabling		2 x 1
Installation/Debugging		3 x 6
Integration	1 x 2	
R & D	1 x 12	1 x 18
Miscellaneous	1 x 2	2 x 18
TOTAL	2 person-year $120 k (@$60k/yr/person)	150 person-months≈12.5 person-year $375 k(@$30k/person/yr)

COST ESTIMATE (cont.)

Scintillation Fibers	: 3HF(1500PPM)+PTP(1%), 0.5 mm, 2.2 meter each (*KURARAY Price List :$0.34/meter)	$0.75*	x 57,000	$ 42.6	k
Clear Fiber	: 0.8 mm, 7.4 meter (**KURARAY Price List : $0.57/meter)	$4.22**	x 57,000	$ 240.4	k
Cassette+VLPC	: D0 style, 1024 channel, assembled	$50,000	x 60	$ 3,000	k
Cryostat/Plumbing	:	$5 / chan	x 57,000	$ 285	k
Support Cylinder	: ROHACELL(#31)+Carbon Fiber Cloth			$ 5	k
Support Structure	:			$ 20	k
Fiber Ribbon Jig	: Grooved Plate	$1.5 k	x 4	$ 6	k
CMM Accessary	:			$ 20	k
Fiber Mounting Jig	:			$ 50	k
Electronics					
SVX II Chips	: 128 chan/chip	$100	x 480	$ 48	k
Port Cards	:	$3 k	x 22	$ 66	k
G-link $ fibers	:			$ 50	k
VME SAR/SRC boards:				$ 25	k
Miscellaneous	:			$ 25	k
Test stand				$ 50	k
Trigger				$ 190	k
Light Pulsing System				$ 66	k
Miscellaneous				$ 50	k
Labor	:			$ 495	k
TOTAL				**$4,784**	**k**

12. Summary

We propose to install a set scintillating fiber tracking layers in the intermediate radial range between SVX II and CTC for Run II. This will not only remedy the inefficiency of the inner superlayers of CTC but furthermore provide a powerful link between SVX II and CTC in a very high luminosity environment expected in Run II.

We envision six layers of axial layers and six layers of stereo layers as a default each consisting of a half-cell staggered layer of 0.5 mm OD scintillating fibers. Preliminary study indicates such a system is quite necessary and adequate.

Thanks to the recent development in technology and CDF's experince through endplug calorimeter upgrade project, the necessary technology and knowledge are in hand to build such a sytem.

Detailed account of the conception of such system is described.

Futher simulation study is necessary to optimize the tracking efficiency. Also an intensive R & D is desirable to optimize the mechanical aspect and finalize the design.

The parameters of the proposed scintillating fiber tracking layers, IFT, are listed in **Table 9**.

Table 9. Intermediate Scintillating Fiber Tracking Layers (IFT) Parameter Summary

Multiclad Fiber Parameters

Outer Cladding	:	Fluorinated PMMA (n=1.42) $\Delta r = 0.03 \times OD$
Inner Cladding	:	PMMA (n=1.49) $\Delta r = 0.03 \times OD$
Sensitive Core	:	Polystyrene (n=1.59) $D = 0.88 \times OD$
Total Int Refl Angle	:	$\cos^{-1}(\frac{1.42}{1.59}) = 26.7°$
Capturing Aperture	:	$\frac{1}{2}(1-\frac{1.42}{1.59}) = 5.35\ \%$

Scintillating Fiber
- Multiclad
- PTP 1%
- 3HF 1500 PPM
- 0.5 mmOD
- 3.1 m

Clear Fiber (Scintillating Fiber - Cryostat Entrance)
- Multiclad
- 5.8 m

Clear Fiber in Cassette
- Multiclad
- 0.9 mm^{OD}

VLPC

Sensitive Window	: 1 mm^{D}
QE	: ≥ 70 %
Gain	: ≥8x 10^4
Noise (≥1 photoelectrons)	: ≤5kHz/sec
Operating Temperature	: 6.5°~7° K

VLPC Chip
- 8 cells/chip
- 1.5 mm x 9.0 mm

Substrate
- 16 chips/substrate = 128 channels/substrate
- 12.5 mm x 50 mm

Cassette
- 8 substrate/cassette = 128 channel/cassette

Tracking Layer Configuration

0.5 mm scintillating Fiber, 0.6 mm Spacing,
Staggered Doublet

References

1) M. Atac, J. Park, D. Cline, D. Chrisman, D. Petroff, and E. Anderson
Nucl. Inst. Meth. A314 (1992) 56.

2) Y. M. Park,
D0 Note

3) B. Baumbaugh, et al.
Nucl. Inst. Meth. A345 (1994) 271

4) G. Appollinari, P. de Barbaro, and M. Mishina,
Proceedings; 4th Int. Conf. on Calorimetry in High Energy Physics,
La Biodola, Isola d'Elba, Italy, 1993, P 200.
P. de Barbaro, et al.,
CDF Note 2778.

5) J. Park, D. Chrisman, M. Atac, and M. Mishina
To be published in IEEE NS proceedings.

6) A. Bros and A. Pla-Dalmau
Nucl. Inst. Meth. Phys. Res. A327(1993)337.
A. Bross, C.L. Kim
Private communication.

7) M. Ching and S. Margulies,
To be published in the Proc. of Scintillating Fiber Workshop
University of Notre Dame, 1993.

8) C. D'Ambrosio, et al.,
Nucl. Inst. Meth. Phys. Sci. A345(1994)279.

9) B. Howell, D. Koltick, C. Cooper, J. Hinson, T. Crone, and D. Michael,
D0 Note 2009.
D. S. Koltick,
To be published in the proceedings of Scintillating Fiber Workshop
University of Notre Dame, 1993. Purdue University Report PU-94-677.

Figure Captions

Fig. 1 Average number of interactions per bunch crossing for various operating conditions.

Fig. 2 Side view of the proposed Scintillating Fiber Tracking Layers (IFT) in the tracking volume.

Fig. 3 Basic composition of the half-spacing staggered doublet layer of 0.5 mm^{OD} scintillating fibers with 0.6 mm spacing. Effective cell size is 0.3 mm.

Fig. 4 Single doublet-layer Z-resolution of stereo layers.

Fig. 5 Dependence of the Z-resolution and the ghost probability on the stereo angle.

Fig. 6 Pulse height spectrum of HISTE IV measured by D0 cosmic ray test[2].

Fig. 7 Quantum efficiency of HISTE's I through IV compared with SSPM.

Fig. 8 Dependence of the quantum efficiency and the noise rate (≥1 pe) on the operating voltage

- a SSPM
- b HISTE V

Fig. 9 Structure of multiclad and single-clad fibers.

Fig. 10 Internal total reflection in multiclad and single clad fibers.

Fig. 11 Microscope photograph of an end of scintillating fiber (3HF) finished with diamond fly-cutter.

Fig. 12 Histograms of the diameter of commercial fibers:

- a 1 mm^{OD} sampled over 16 km.
- b 0.830 mm^{OD} sampled over 20 km.

Fig. 13 Histogram of light output from waveshifter doped fibers sampled at every 150 meter over the total of 16 km used for the production of E.M. section of the new end plug calorimeter. ~70-cm long Y-11 waveshifter fibers were inseterd into a scintillator tile with Sr90 souce as the light source and the output from 30-cm long tail out of the tile is measured by a phototube.

Fig. 14 Reflectivity of mirrored ends of the fibers[4] sampled over the production period of the hadronic section tile/fiber assemblies. Cross hatched histogram corresponds to the data taken when the aluminum spattering vessel was contaminated.

Fig. 15 R-ϕ cross sectional views of the proposed intermediate scintillating fiber tracking layers.

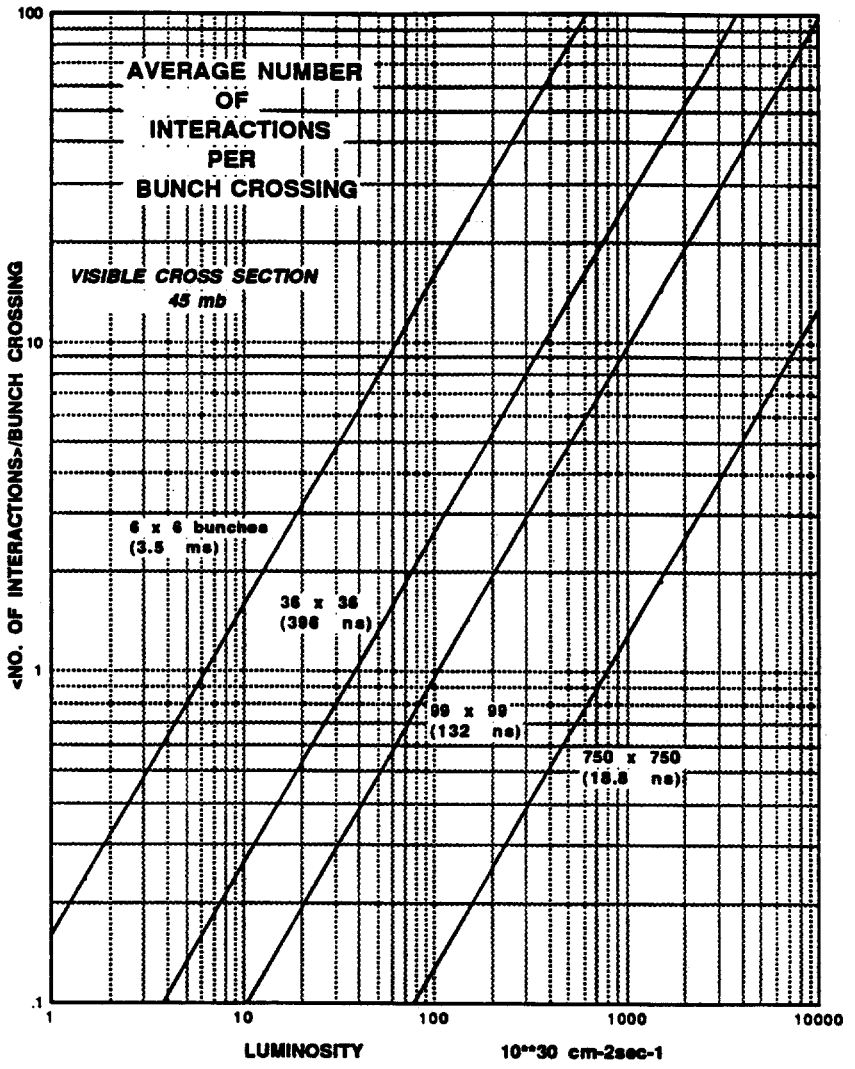
AVERAGE NUMBER
OF
INTERACTIONS
PER
BUNCH CROSSING
VISIBLE CROSS SECTION
45 mb
6 x 6 bunches
(3.5 ms)
36 x 36
(396 ns)
99 x 99
(132 ns)
750 x 750
(18.8 ns)
<NO. OF INTERACTIONS>/BUNCH CROSSING
100
10
1
.1
1
10
100
1000
10000
LUMINOSITY
10**30 cm-2sec-1

Fig. 1

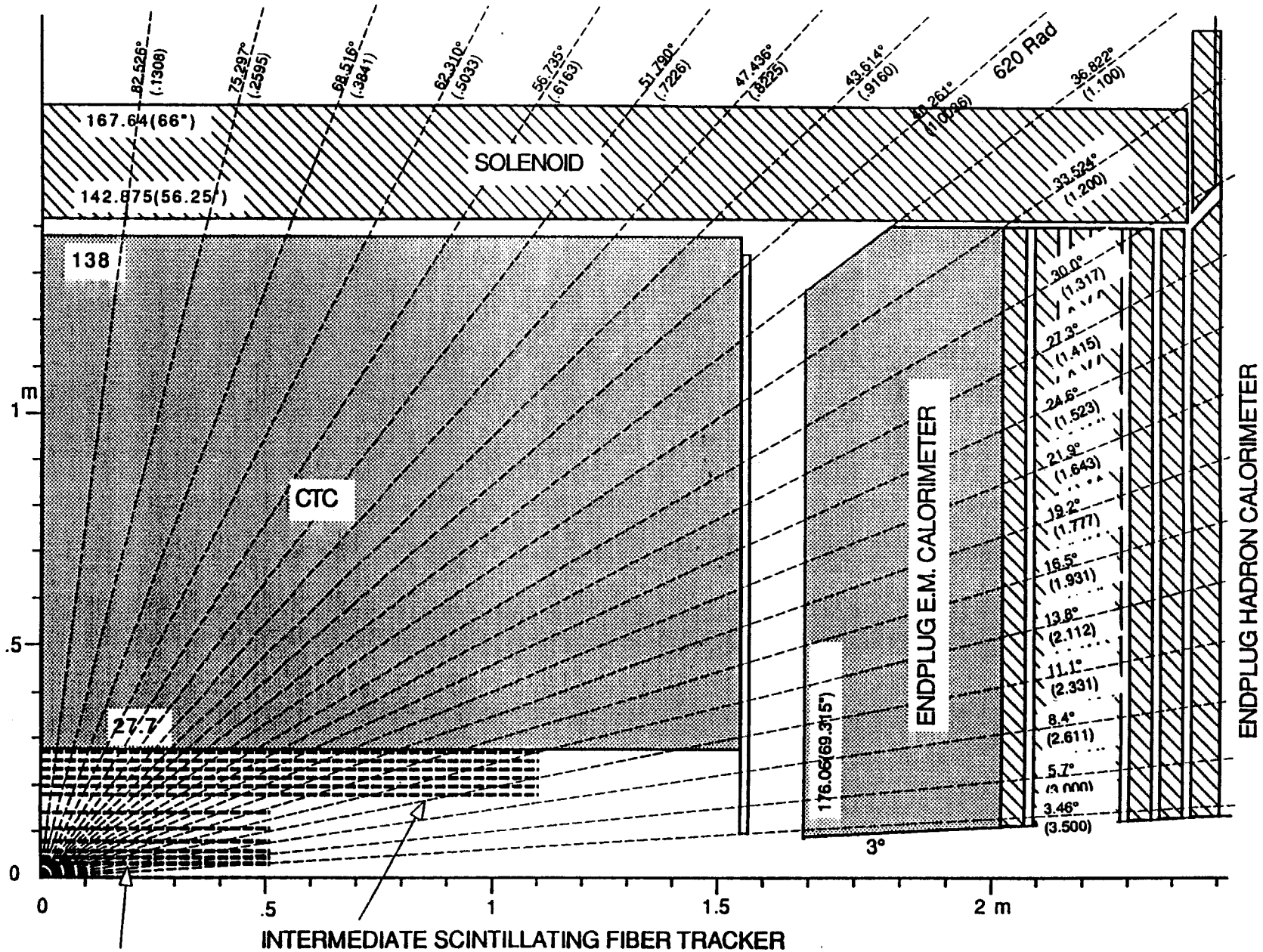
82.526° (.1308)
75.297° (.2595)
68.516° (.3841)
62.310° (.5033)
56.735° (.6163)
51.790° (.7226)
47.436° (.8225)
43.614° (.9160)
40.261° (1.0036)
620 Rad
36.822° (1.100)
33.524° (1.200)
167.64(66")
142.875(56.25")
SOLENOID
138
CTC
27.7
176.06(69.315")
ENDPLUG E.M. CALORIMETER
30.0° (1.317)
27.3° (1.415)
24.6° (1.523)
21.9° (1.643)
19.2° (1.777)
16.5° (1.931)
13.8° (2.112)
11.1° (2.331)
8.4° (2.611)
5.7° (3.000)
3.46° (3.500)
3°
ENDPLUG HADRON CALORIMETER
1 m
.5
0
0
.5
1
1.5
2 m
INTERMEDIATE SCINTILLATING FIBER TRACKER
SVX II

Fig. 2

0.5 mm OD ROUND FIBER

MULTICLAD FIBER
INNER CLAD O.D. : 0.94 O.D.
CORE OD : 0.88 O.D.

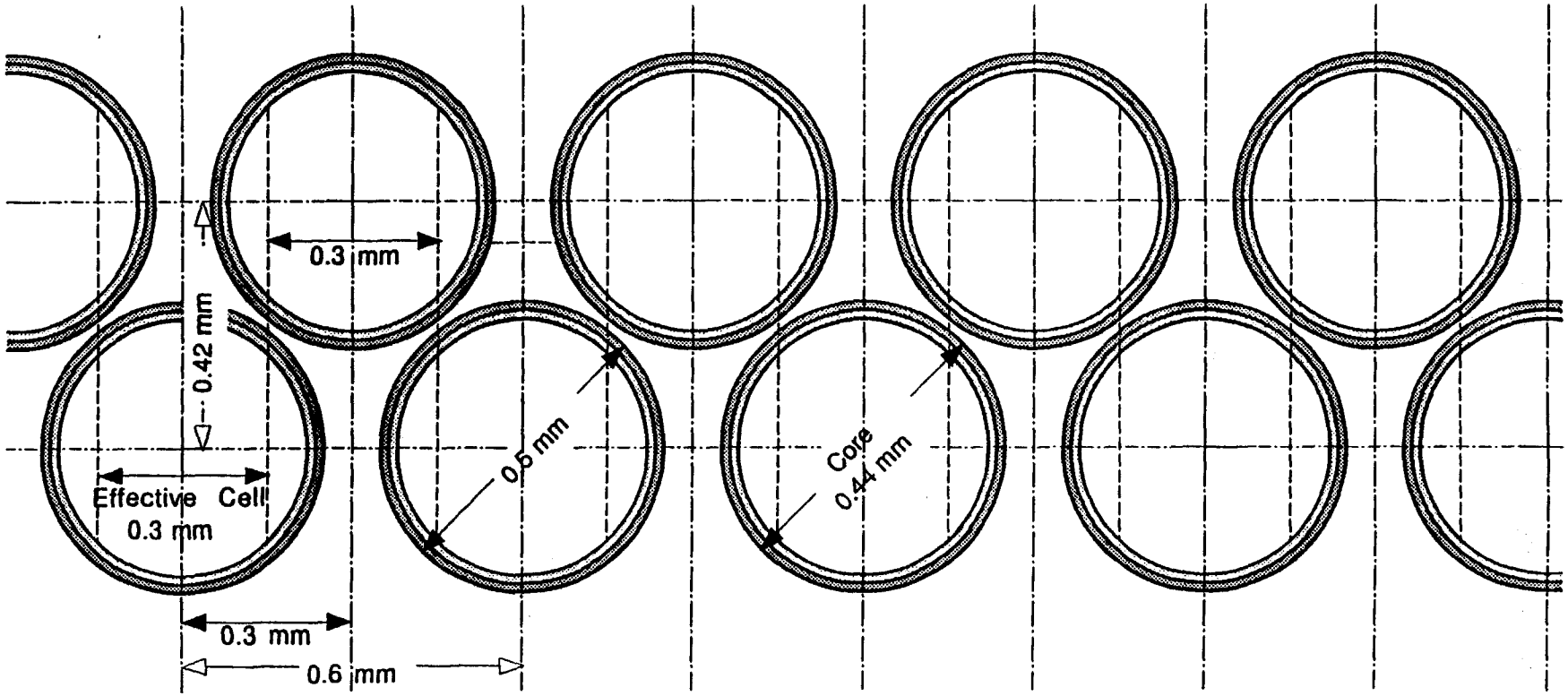

σ intrinsic $= \frac{0.3 \text{ mm}}{\sqrt{12}} = 86.6 \ \mu m$

σ total = 86.6 $\oplus$ 25 = 90.1 μm

Average Thickness = (π/4) 0.5 mm x 2*/1.2** = 0.6545 mm

Fig 3

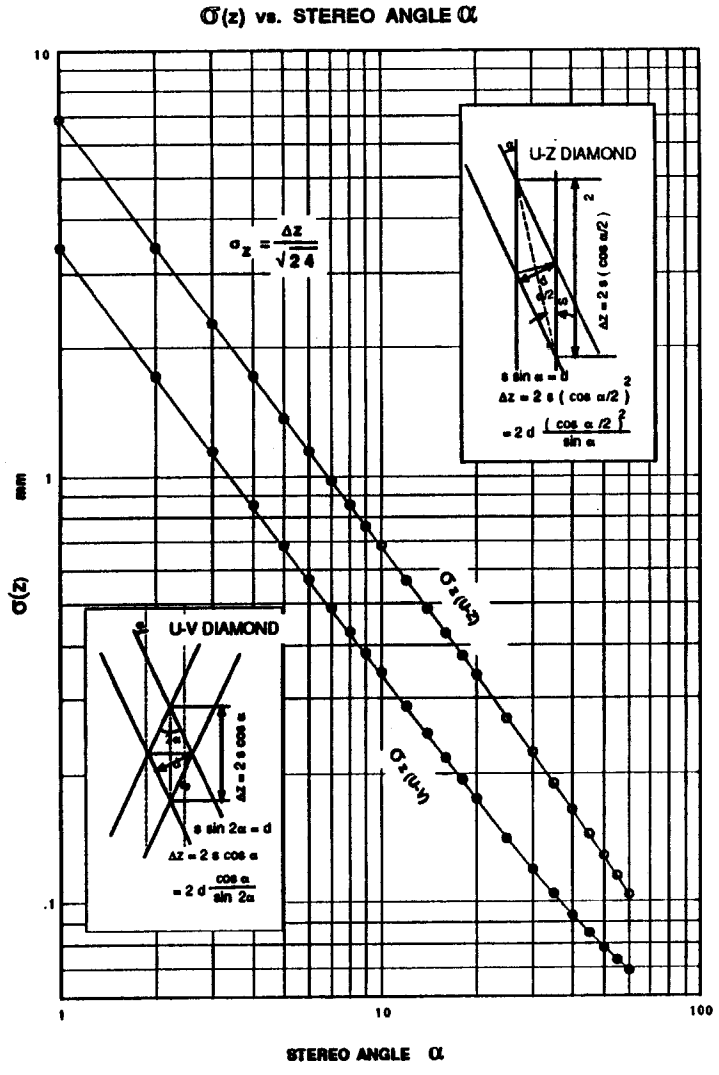
σ(z) vs. STEREO ANGLE α
σ(z) mm
STEREO ANGLE α
U-Z DIAMOND
U-V DIAMOND
10
1
.1
1
10
100

Fig. 4

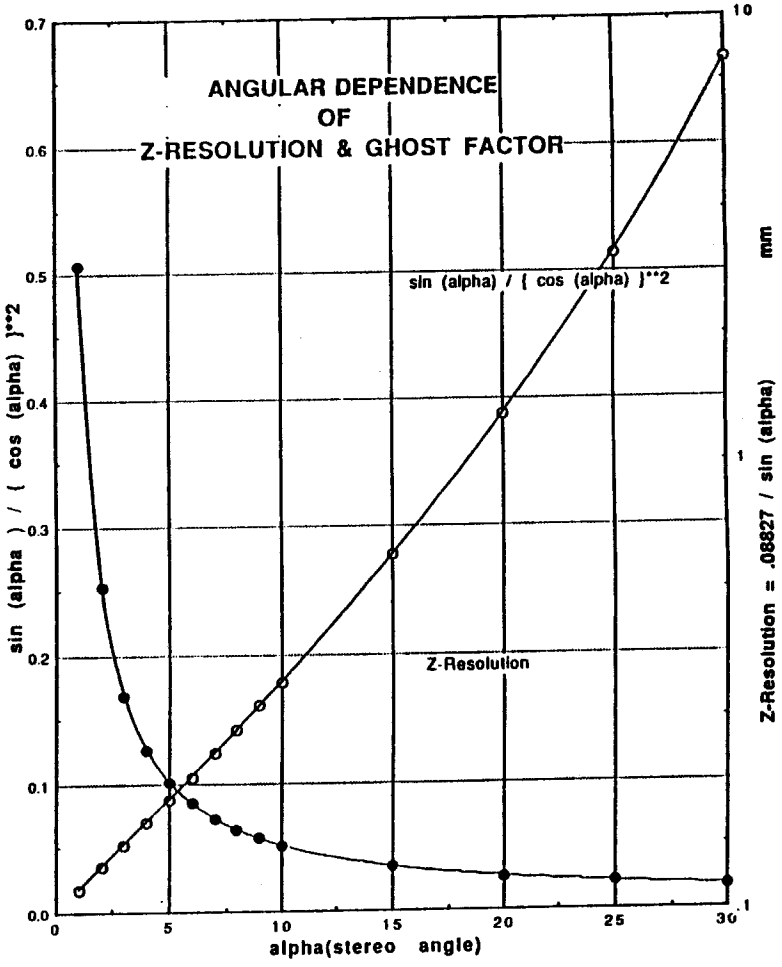
ANGULAR DEPENDENCE
OF
Z-RESOLUTION & GHOST FACTOR
sin (alpha) / (cos (alpha))**2
Z-Resolution
sin (alpha) / (cos (alpha))**2
Z-Resolution = .08827 / sin (alpha)
mm
alpha(stereo angle)
0.0
0.1
0.2
0.3
0.4
0.5
0.6
0.7
0
5
10
15
20
25
30
1
10

Fig.5

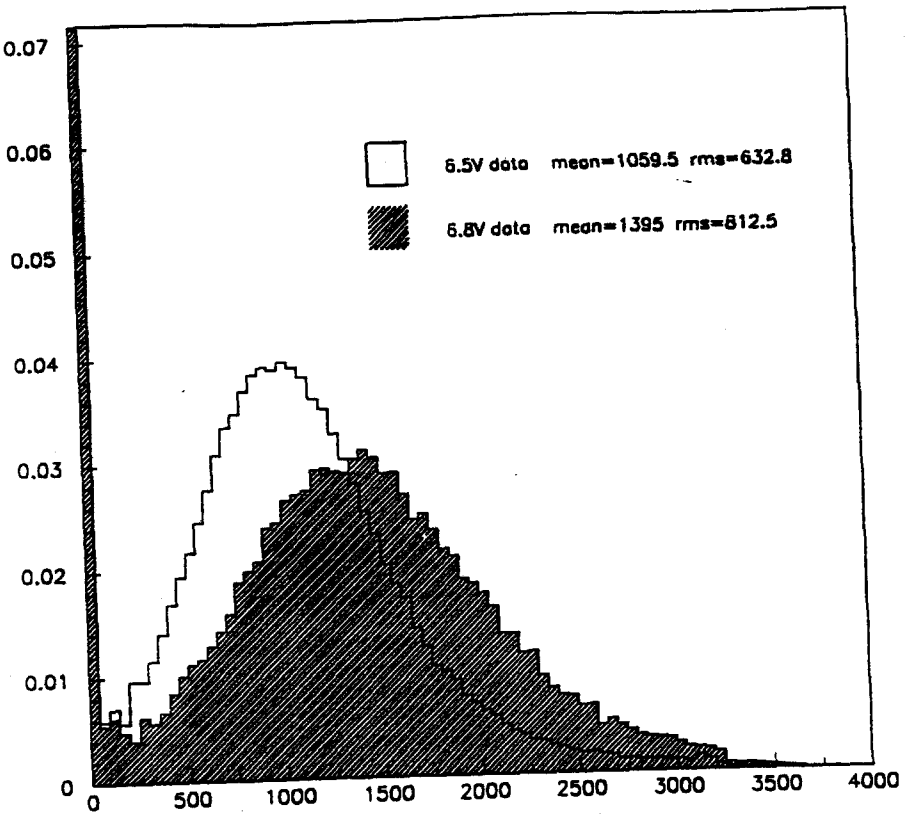
0.07
0.06
0.05
0.04
0.03
0.02
0.01
0
0
500
1000
1500
2000
2500
3000
3500
4000
6.5V data mean=1059.5 rms=632.8
6.8V data mean=1395 rms=812.5

Fig.6

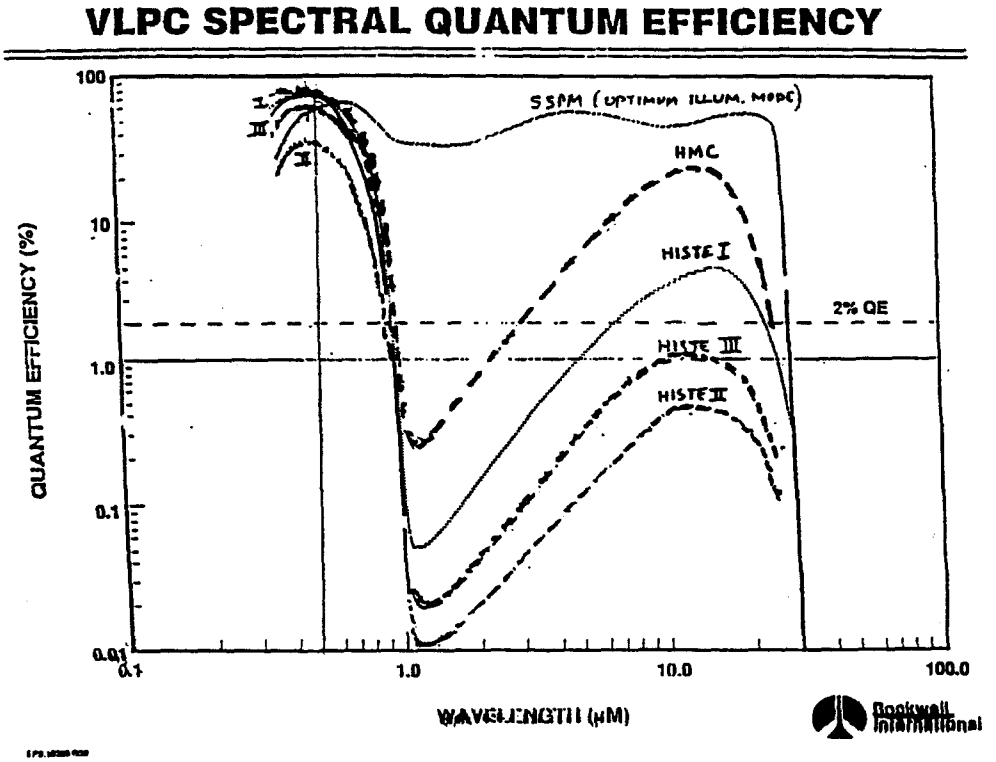
VLPC SPECTRAL QUANTUM EFFICIENCY
QUANTUM EFFICIENCY (%)
100
10
1.0
0.1
0.01
0.1
1.0
10.0
100.0
WAVELENGTH (μM)
SSPM (OPTIMUM ILLUM. MODE)
HMC
HISTE I
HISTE III
HISTE II
2% QE
I
III
II
Rockwell International

Fig.7

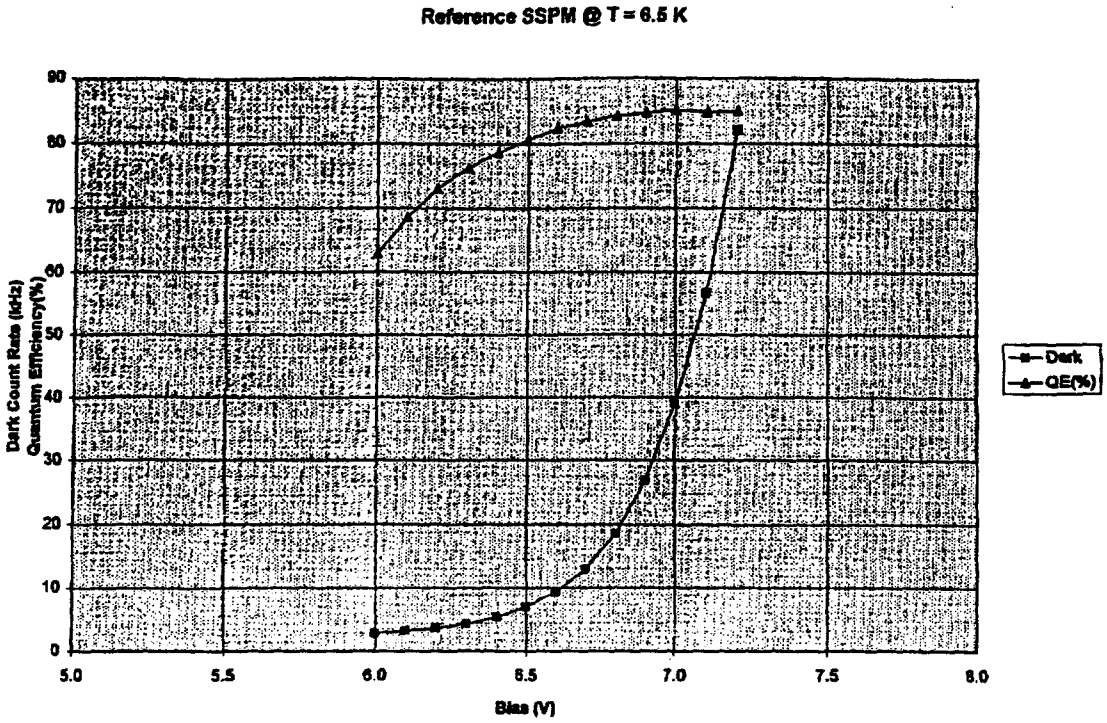
Reference SSPM @ T = 6.5 K
Dark Count Rate (kHz)
Quantum Efficiency(%)
90
80
70
60
50
40
30
20
10
0
5.0
5.5
6.0
6.5
7.0
7.5
8.0
Bias (V)
Dark
QE(%)

Fig.8 a

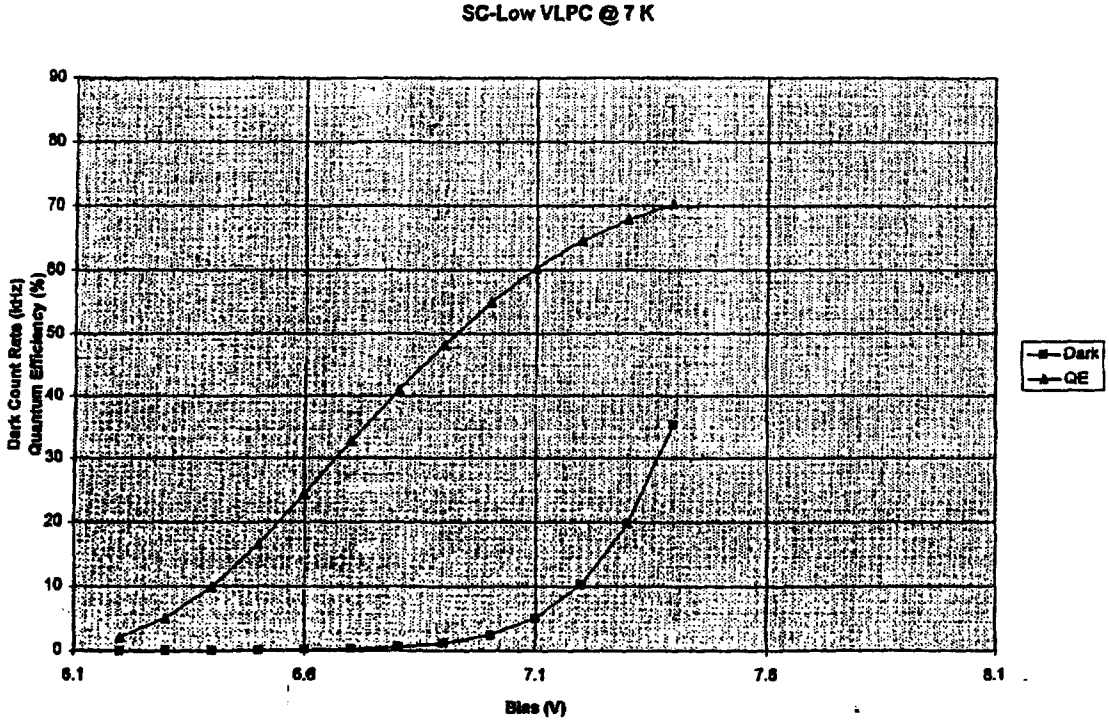
SC-Low VLPC @ 7 K
Dark Count Rate (kHz)
Quantum Efficiency (%)
90
80
70
60
50
40
30
20
10
0
6.1
6.6
7.1
7.6
8.1
Bias (V)
Dark
QE

Fig.8 b

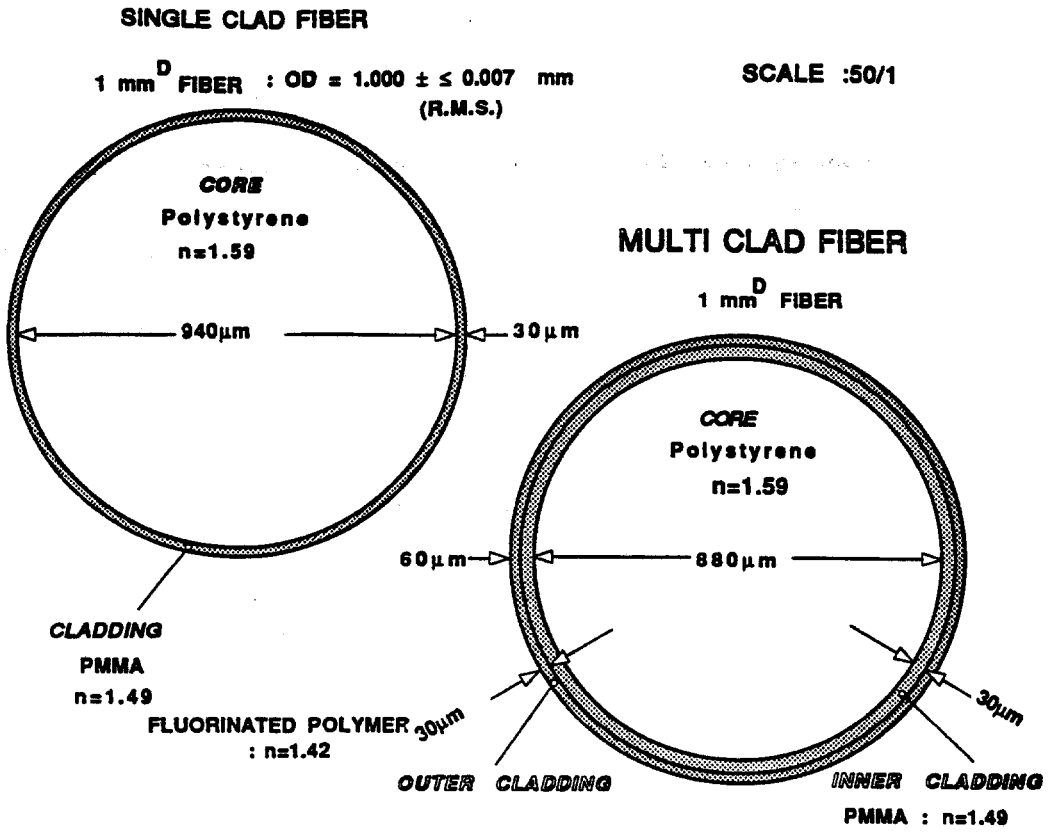
SINGLE CLAD FIBER
1 mm D FIBER : OD = 1.000 ± ≤ 0.007 mm
(R.M.S.)
SCALE :50/1
CORE
Polystyrene
n=1.59
940μm
30μm
CLADDING
PMMA
n=1.49
FLUORINATED POLYMER
: n=1.42
30μm
MULTI CLAD FIBER
1 mm D FIBER
CORE
Polystyrene
n=1.59
60μm
880μm
30μm
OUTER CLADDING
INNER CLADDING
PMMA : n=1.49

Fig.9

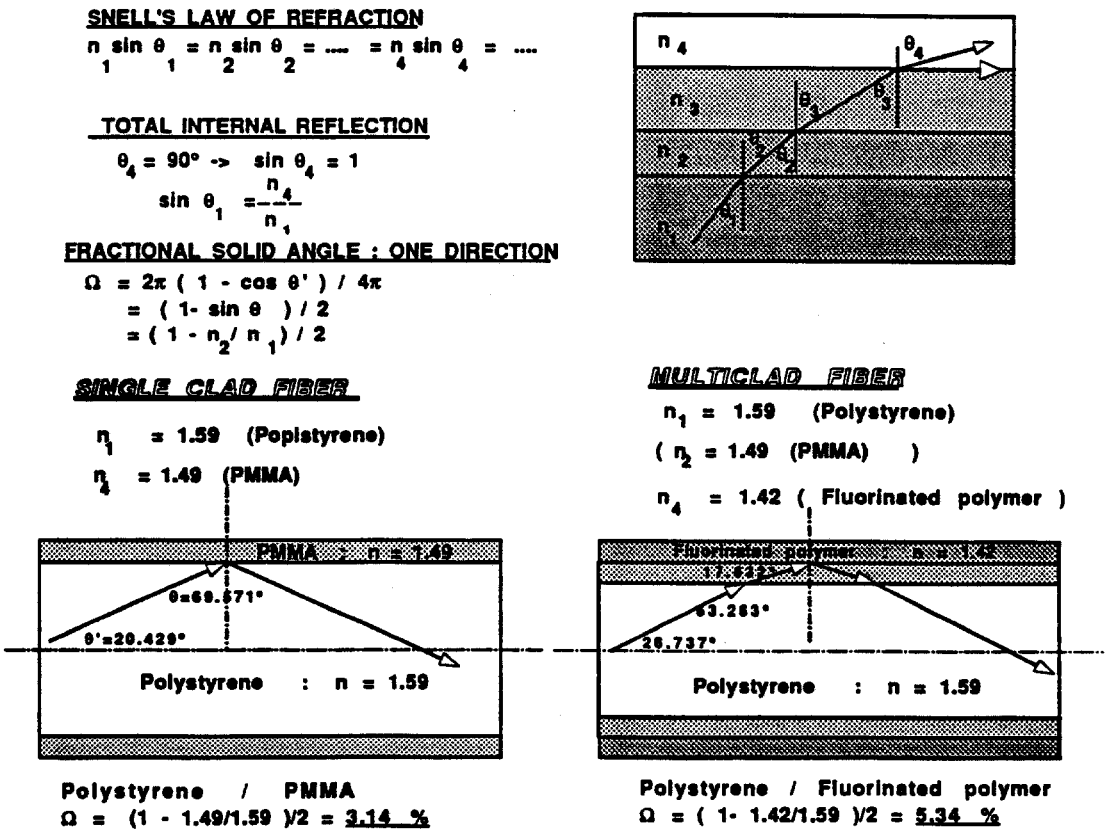
SNELL'S LAW OF REFRACTION
n sin θ = n sin θ = ... = n sin θ = ...
1 1 2 2 4 4
TOTAL INTERNAL REFLECTION
θ4 = 90° -> sin θ4 = 1
sin θ1 = n4 / n1
FRACTIONAL SOLID ANGLE : ONE DIRECTION
Ω = 2π (1 - cos θ') / 4π
= (1- sin θ) / 2
= (1 - n2 / n1) / 2
SINGLE CLAD FIBER
n1 = 1.59 (Popistyrene)
n4 = 1.49 (PMMA)
PMMA : n = 1.49
θ=69.671°
θ'=20.429°
Polystyrene : n = 1.59
Polystyrene / PMMA
Ω = (1 - 1.49/1.59)/2 = 3.14 %
MULTICLAD FIBER
n1 = 1.59 (Polystyrene)
(n2 = 1.49 (PMMA))
n4 = 1.42 (Fluorinated polymer)
Fluorinated polymer : n = 1.42
63.263°
26.737°
Polystyrene : n = 1.59
Polystyrene / Fluorinated polymer
Ω = (1- 1.42/1.59)/2 = 5.34 %

Fig.10

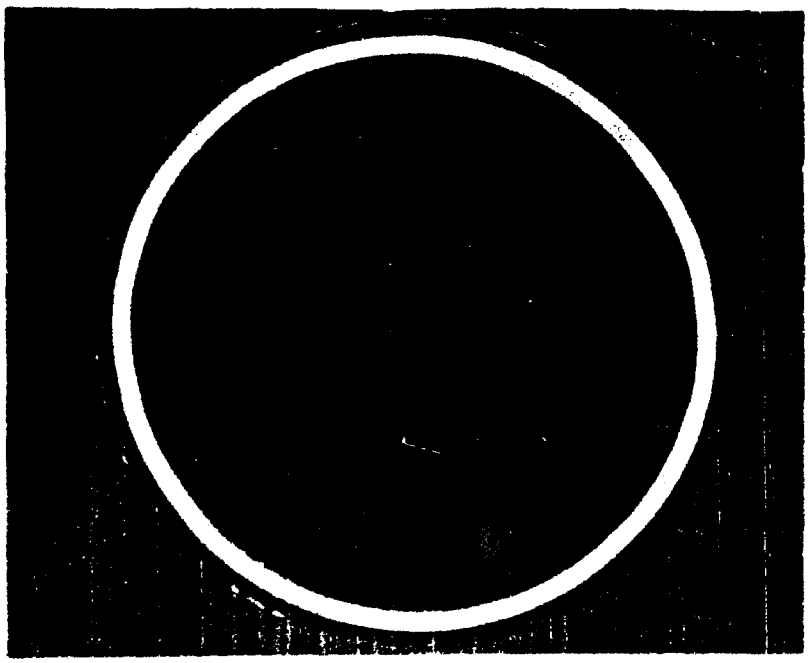

Fig.11

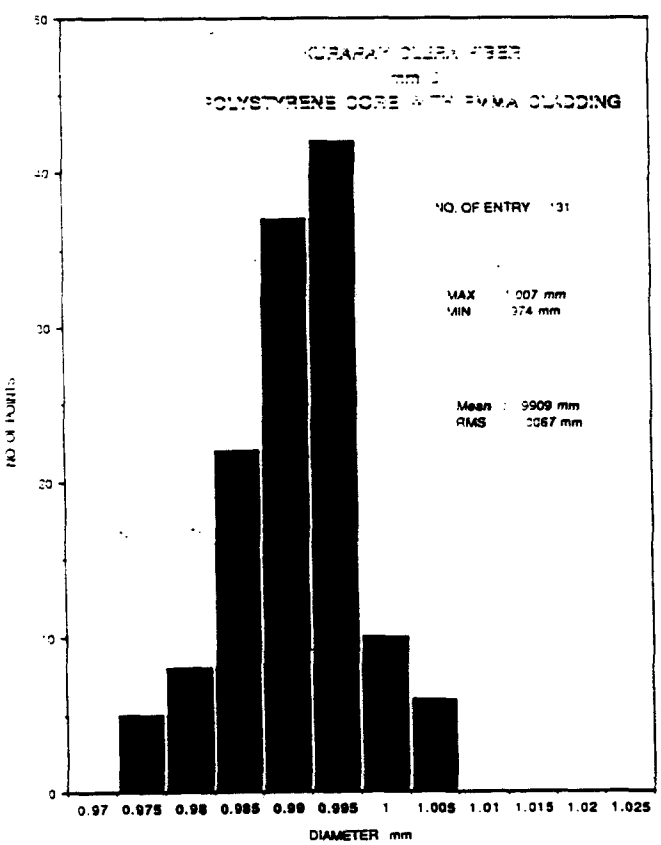

Fig.12 a

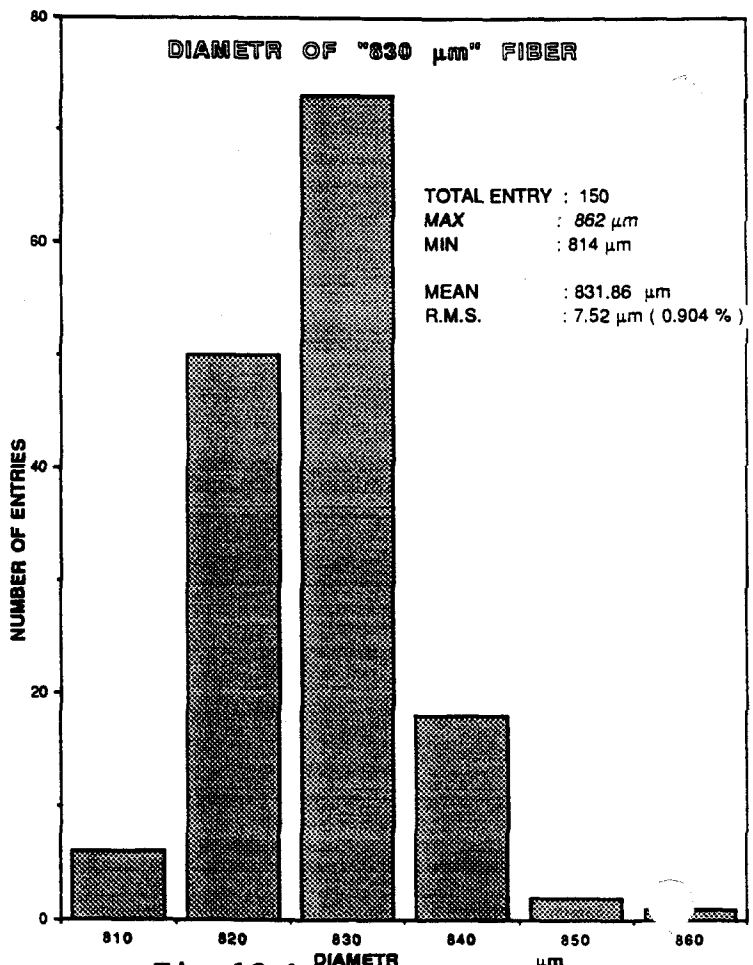

Fig.12 b

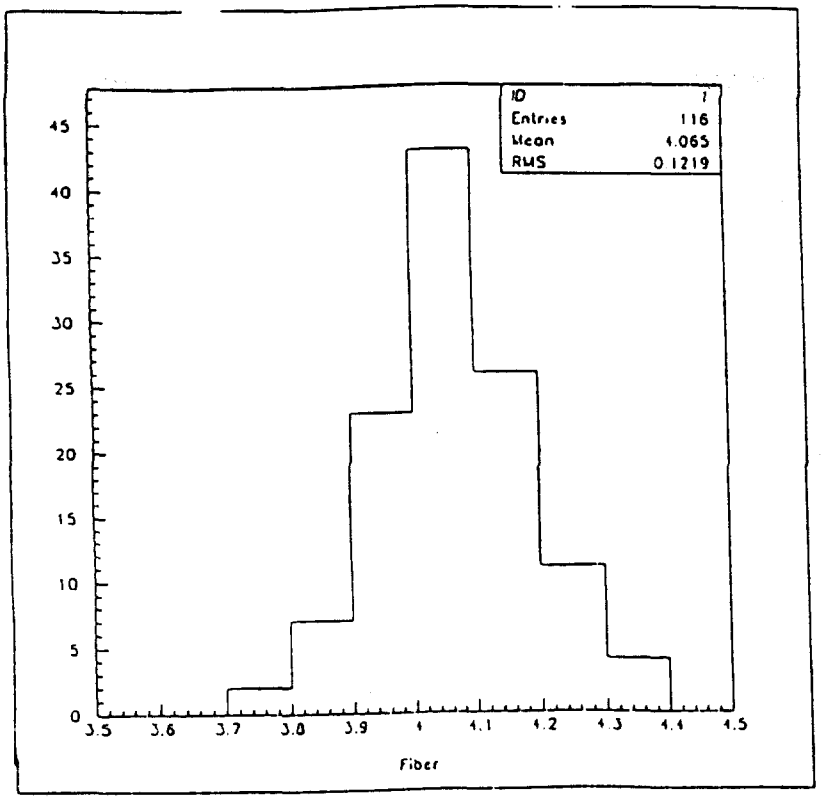
ID 1
Entries 116
Mean 4.065
RMS 0.1219
45
40
35
30
25
20
15
10
5
0
3.5
3.6
3.7
3.8
3.9
4
4.1
4.2
4.3
4.4
4.5
Fiber

Fig.13

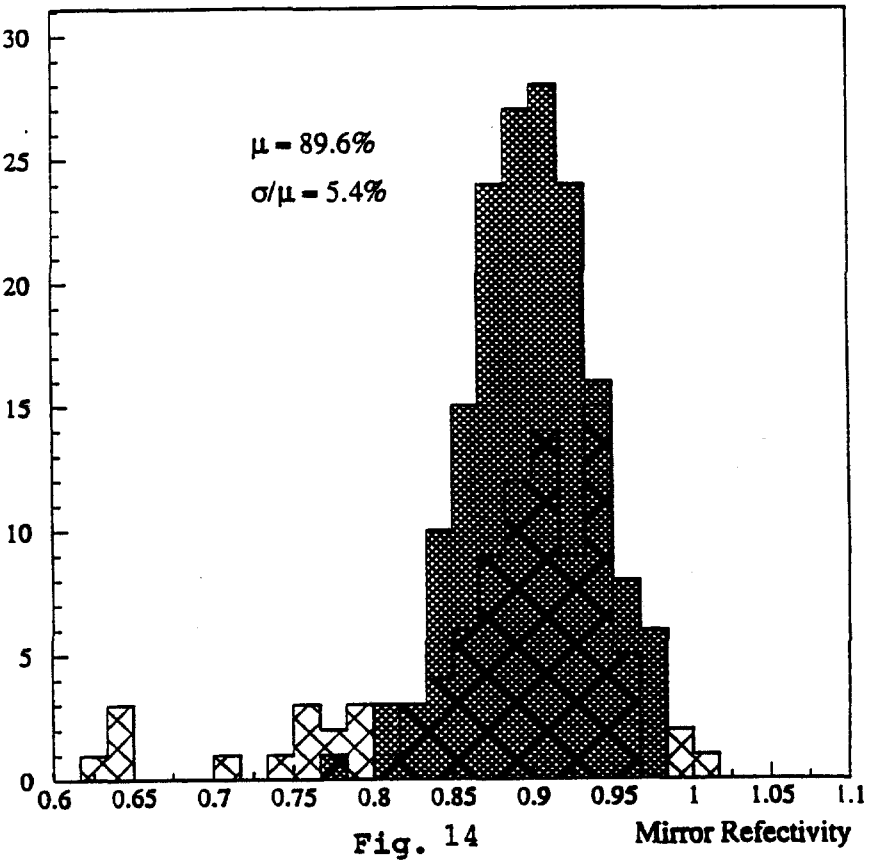
μ = 89.6%
σ/μ = 5.4%
30
25
20
15
10
5
0
0.6
0.65
0.7
0.75
0.8
0.85
0.9
0.95
1
1.05
1.1
Mirror Refectivity

Fig. 14

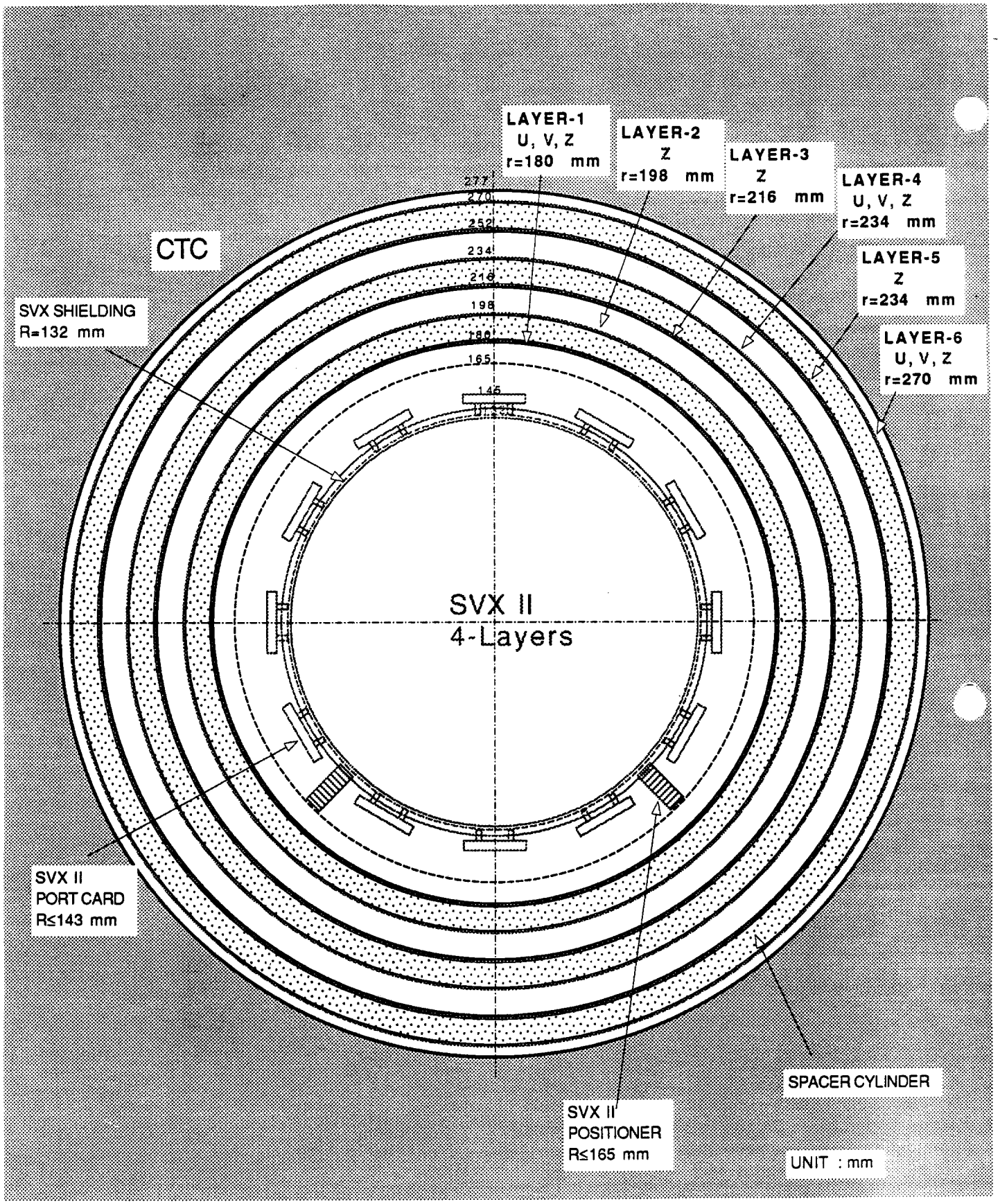
LAYER-1
U, V, Z
r=180 mm
LAYER-2
Z
r=198 mm
LAYER-3
Z
r=216 mm
LAYER-4
U, V, Z
r=234 mm
LAYER-5
Z
r=234 mm
LAYER-6
U, V, Z
r=270 mm
CTC
SVX SHIELDING
R=132 mm
277
270
252
234
216
198
180
165
146
SVX II
4-Layers
SVX II
PORT CARD
R≤143 mm
SPACER CYLINDER
SVX II
POSITIONER
R≤165 mm
UNIT : mm

Fig. 15 a

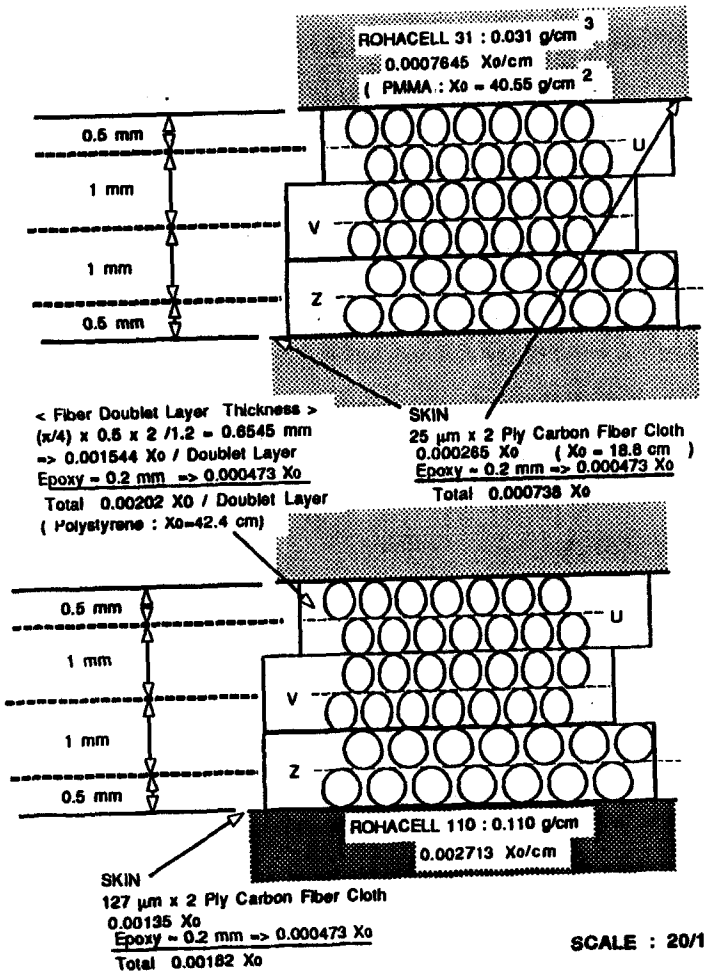

Fig.15 b

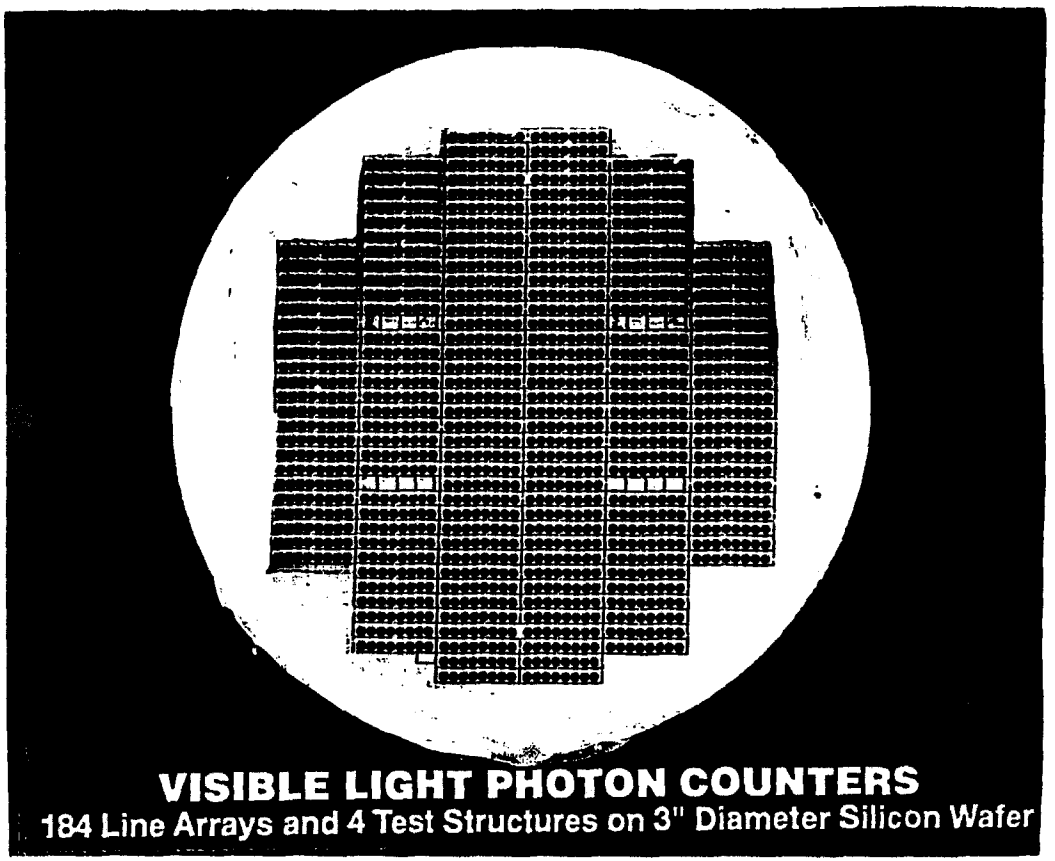

Fig. 16

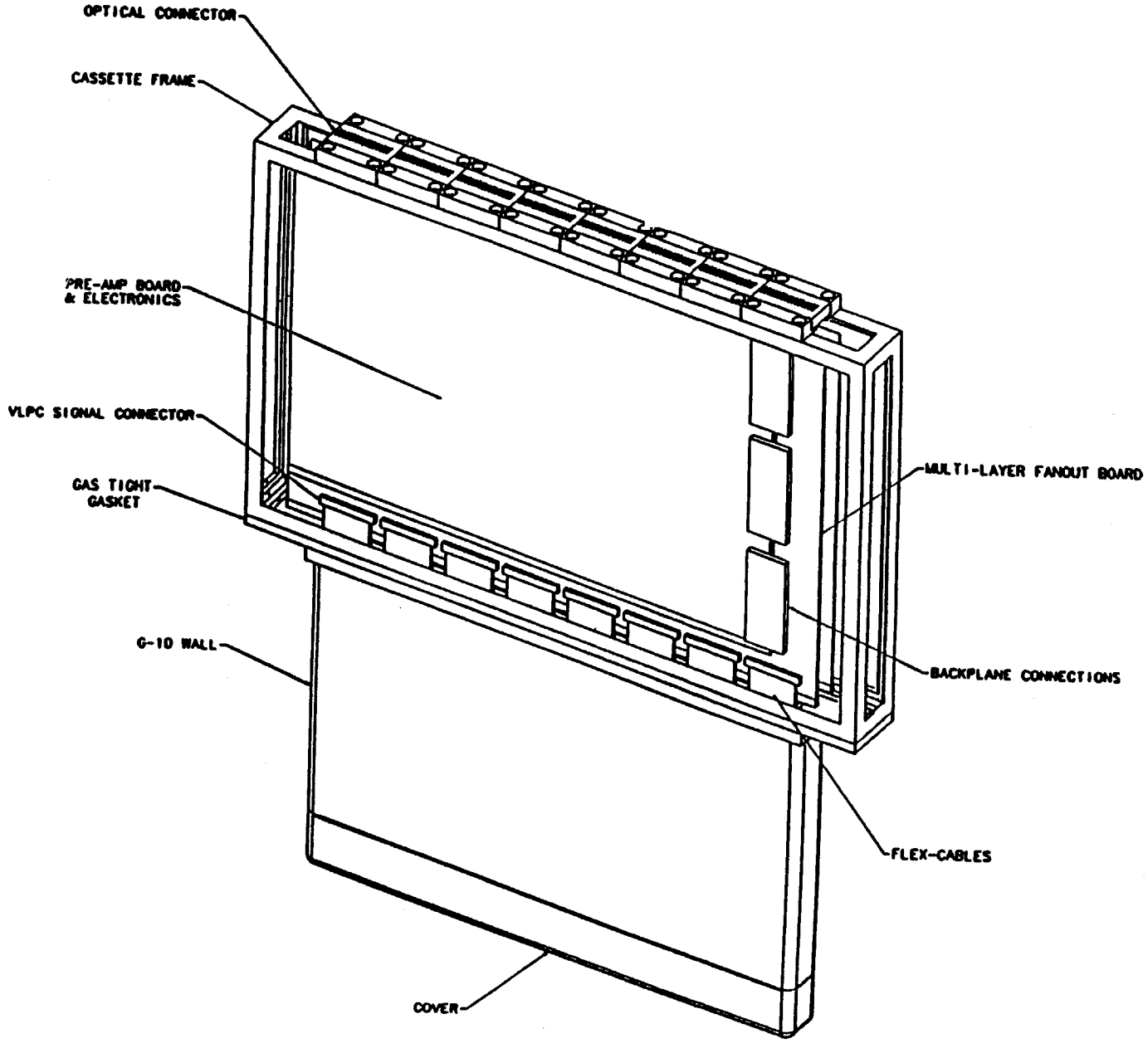

FIGURE #2: OVERALL CASSETTE LAYOUT

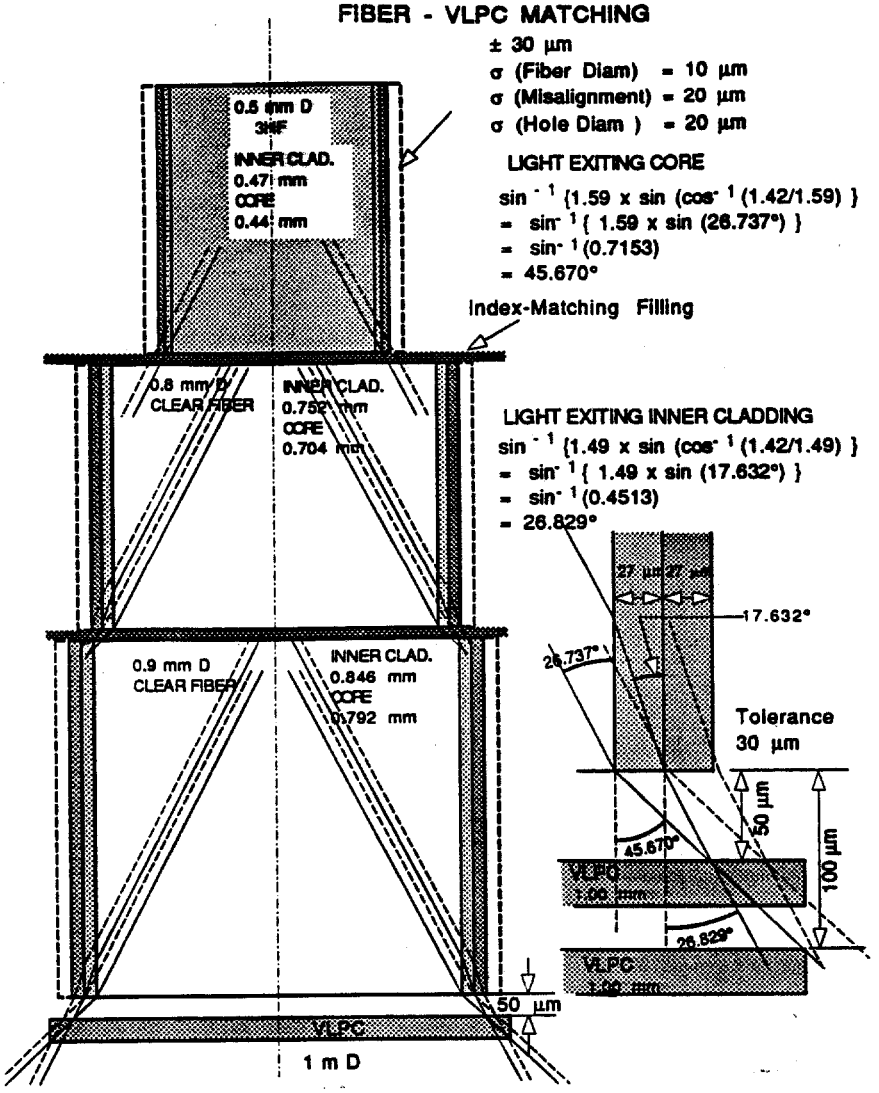
FIBER - VLPC MATCHING
± 30 µm
σ (Fiber Diam) = 10 µm
σ (Misalignment) = 20 µm
σ (Hole Diam) = 20 µm
LIGHT EXITING CORE
sin⁻¹ {1.59 x sin (cos⁻¹ (1.42/1.59) }
= sin⁻¹ { 1.59 x sin (26.737°) }
= sin⁻¹ (0.7153)
= 45.670°
Index-Matching Filling
0.5 mm D
3HF
INNER CLAD.
0.47 mm
CORE
0.44 mm
0.8 mm D
CLEAR FIBER
INNER CLAD.
0.752 mm
CORE
0.704 mm
LIGHT EXITING INNER CLADDING
sin⁻¹ {1.49 x sin (cos⁻¹ (1.42/1.49) }
= sin⁻¹ { 1.49 x sin (17.632°) }
= sin⁻¹ (0.4513)
= 26.829°
0.9 mm D
CLEAR FIBER
INNER CLAD.
0.846 mm
CORE
0.792 mm
17.632°
26.737°
Tolerance
30 µm
50 µm
45.670°
100 µm
VLPC
1.00 mm
26.829°
VLPC
1.00 mm
50 µm
VLPC
1 m D

Fig. 18

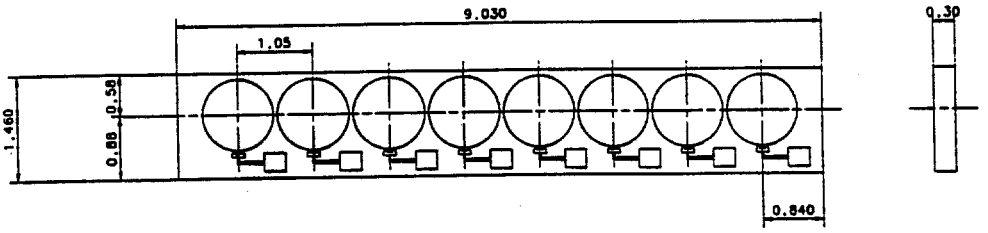
9.030
1.05
1.460
0.58
0.88
0.840
0.30

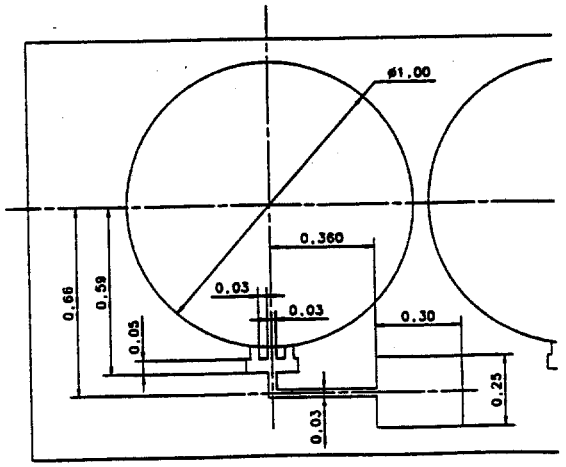
ø1.00
0.360
0.03
0.03
0.30
0.66
0.59
0.05
0.23
0.03

Fig. 19

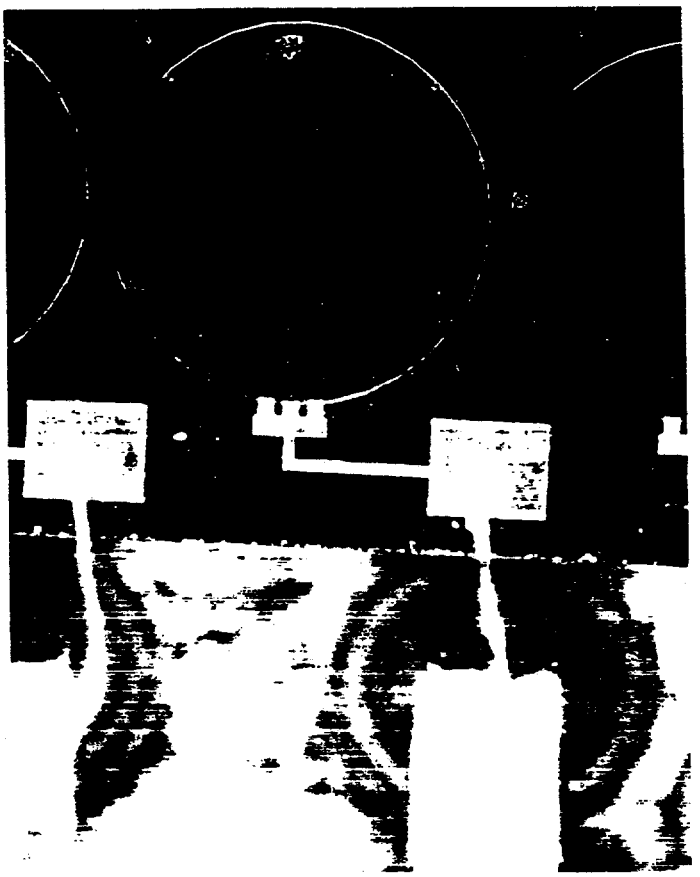

Fig. 20

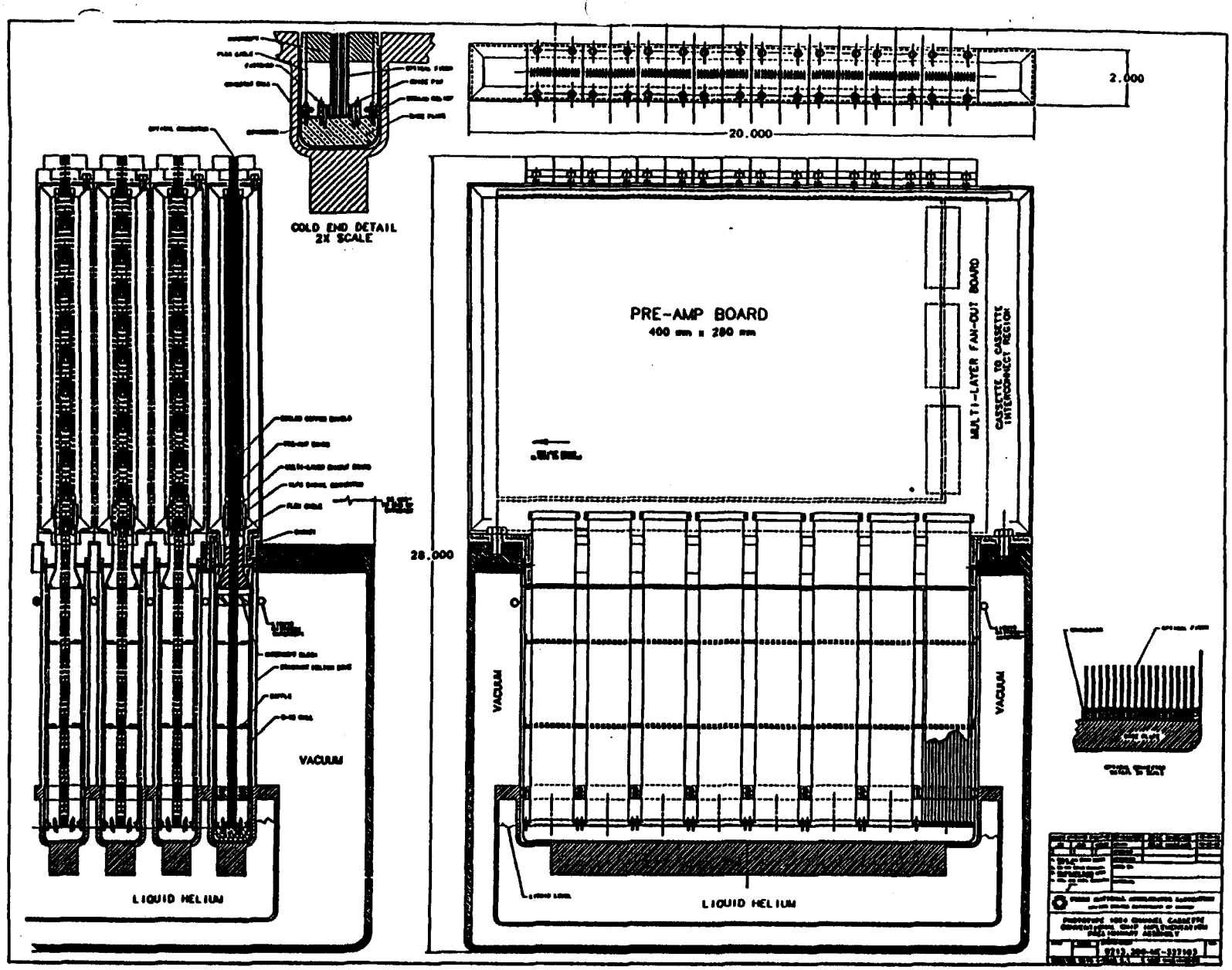

FIGURE #3: PRELIMINARY ASSEMBLY OF CASSETTE

Fig. 21

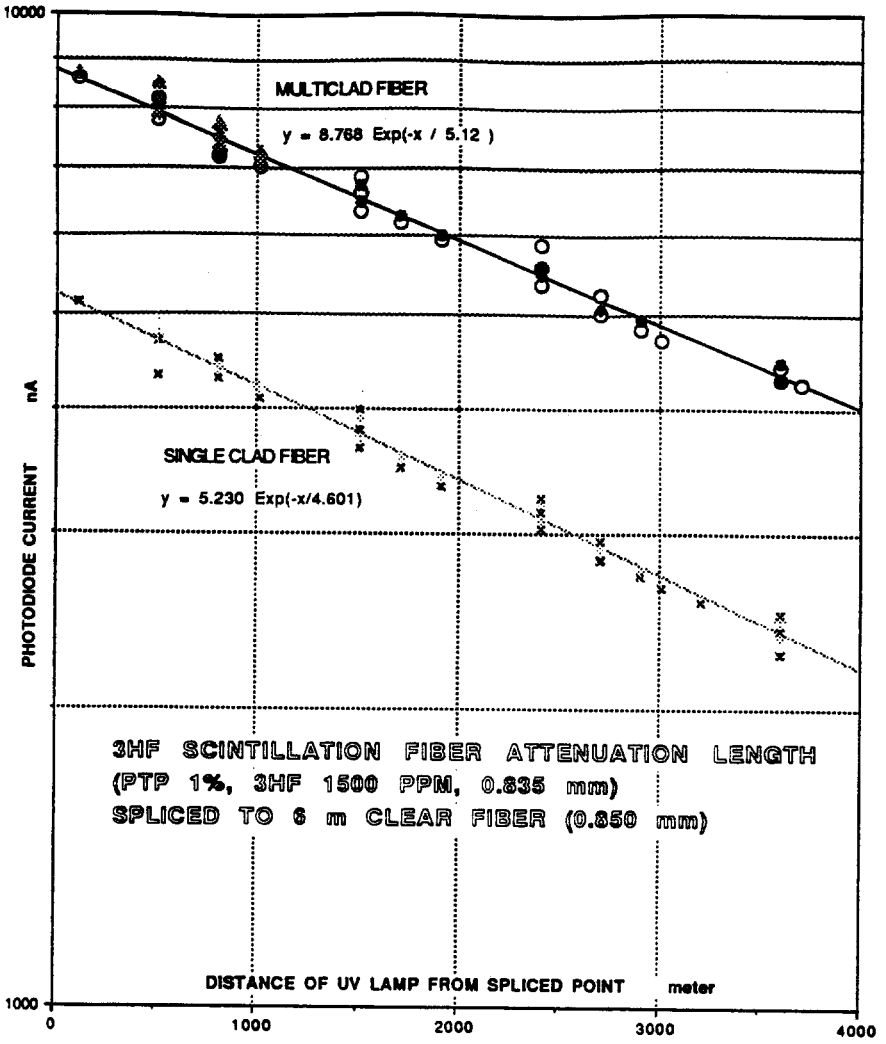

Fig. 22 a

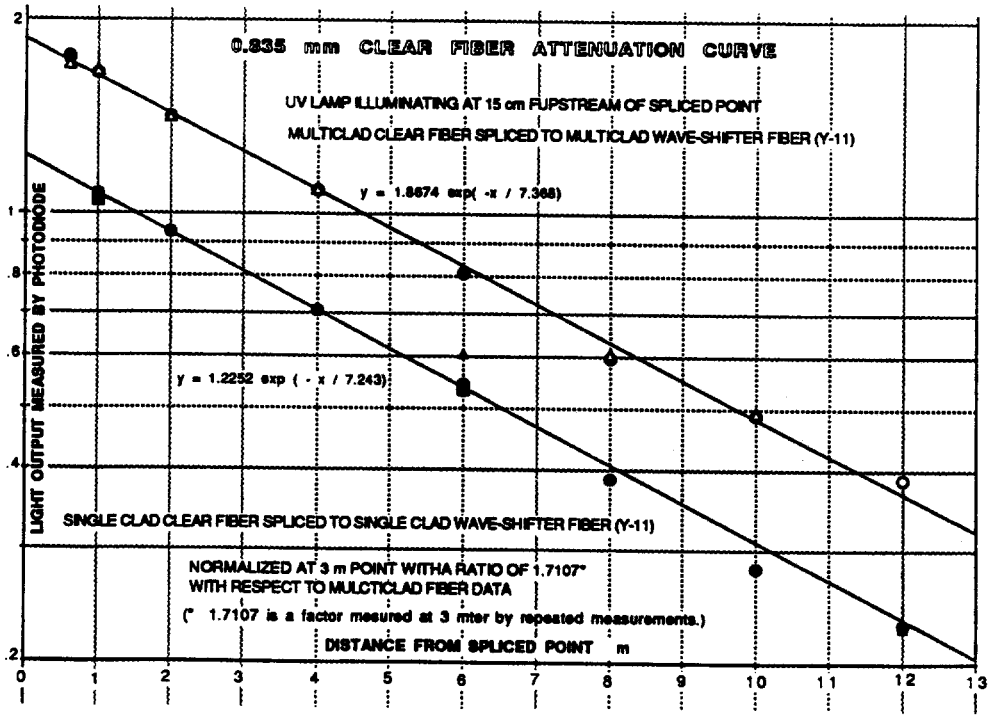

Fig. 22 b

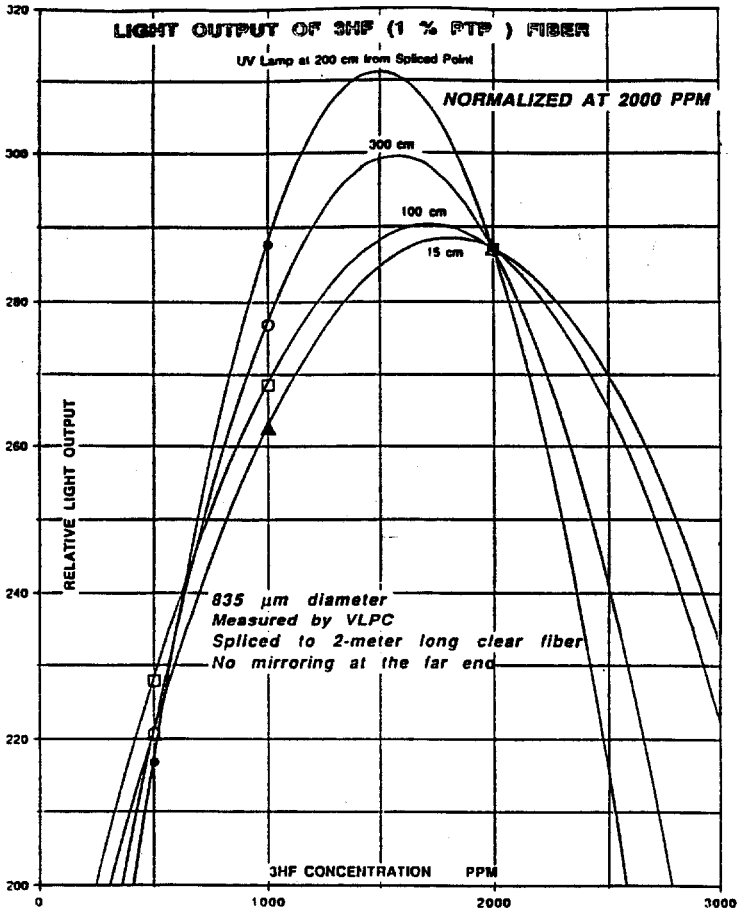
LIGHT OUTPUT OF 3HF (1 % PTP) FIBER
UV Lamp at 200 cm from Spliced Point
NORMALIZED AT 2000 PPM
300 cm
100 cm
15 cm
RELATIVE LIGHT OUTPUT
835 μm diameter
Measured by VLPC
Spliced to 2-meter long clear fiber
No mirroring at the far end
3HF CONCENTRATION PPM
320
300
280
260
240
220
200
0
1000
2000
3000

Fig. 23

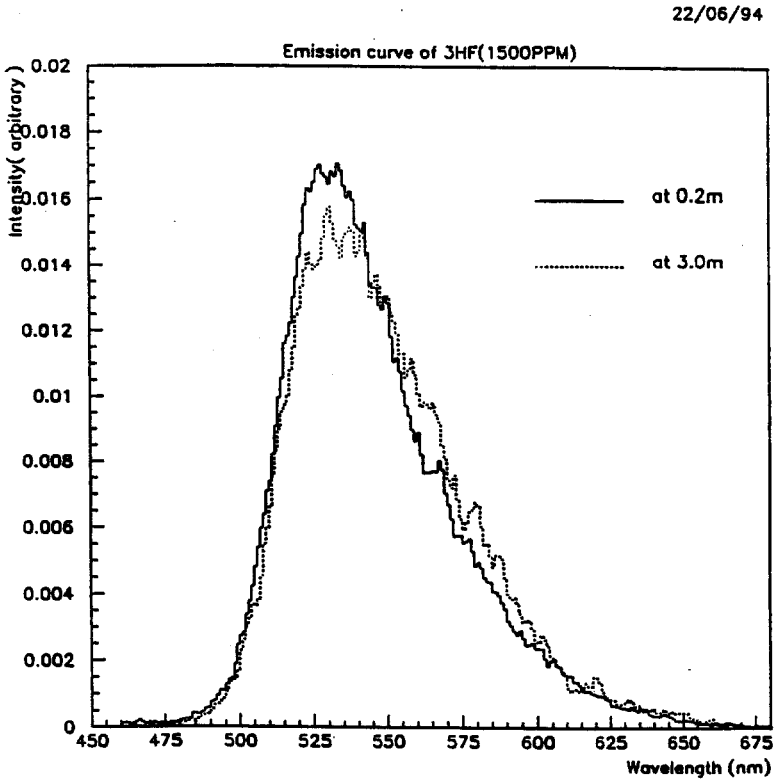
22/06/94 12.51
Emission curve of 3HF(1500PPM)
Intensity(arbitrary)
at 0.2m
at 3.0m
0.02
0.018
0.016
0.014
0.012
0.01
0.008
0.006
0.004
0.002
0
450
475
500
525
550
575
600
625
650
675
Wavelength (nm)

Fig.24

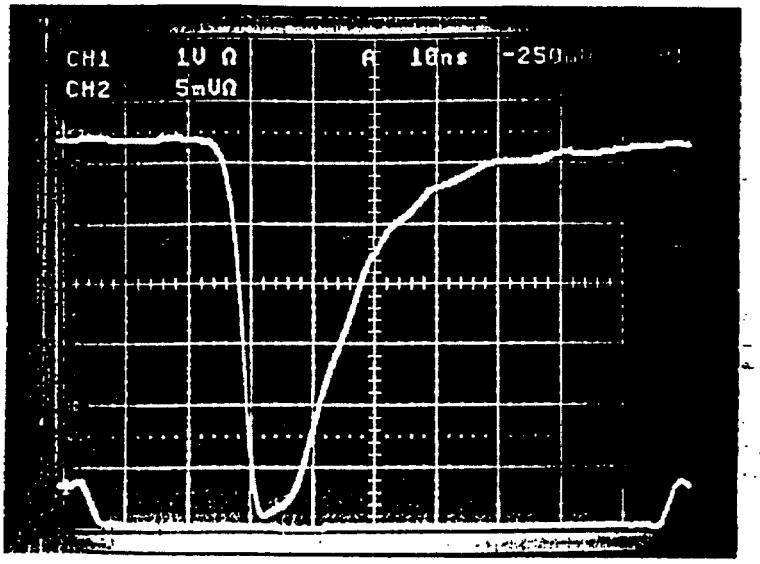

Fig. 25 a

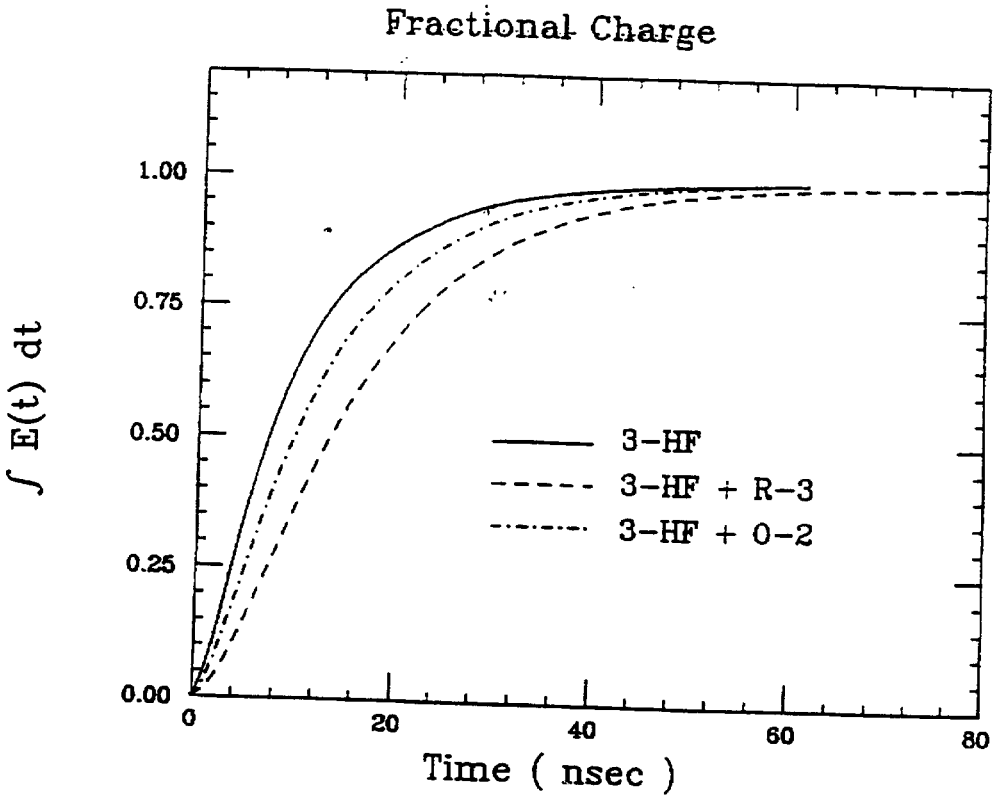

Fig. 25 b

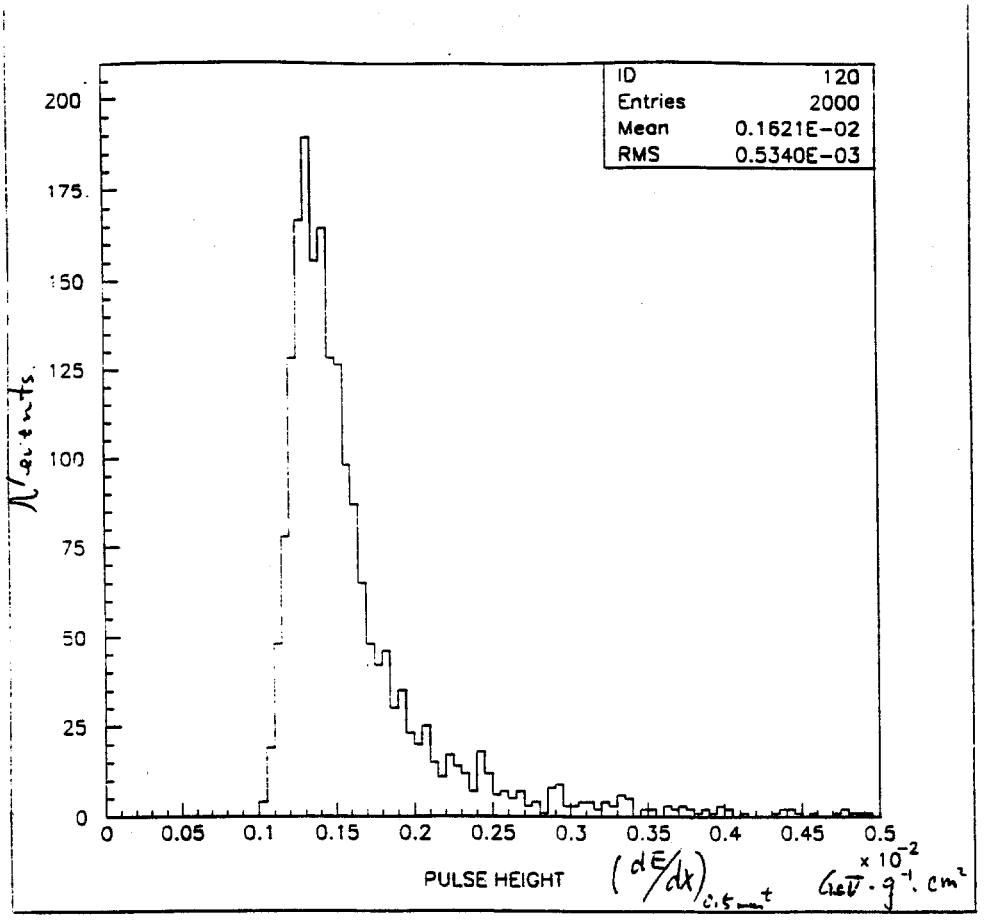
ID 120
Entries 2000
Mean 0.1621E-02
RMS 0.5340E-03
Counts
PULSE HEIGHT
$(dE/dx)_{c.t.}$
$\times 10^{-2}$
GeV · g⁻¹ · cm²

Fig. 26

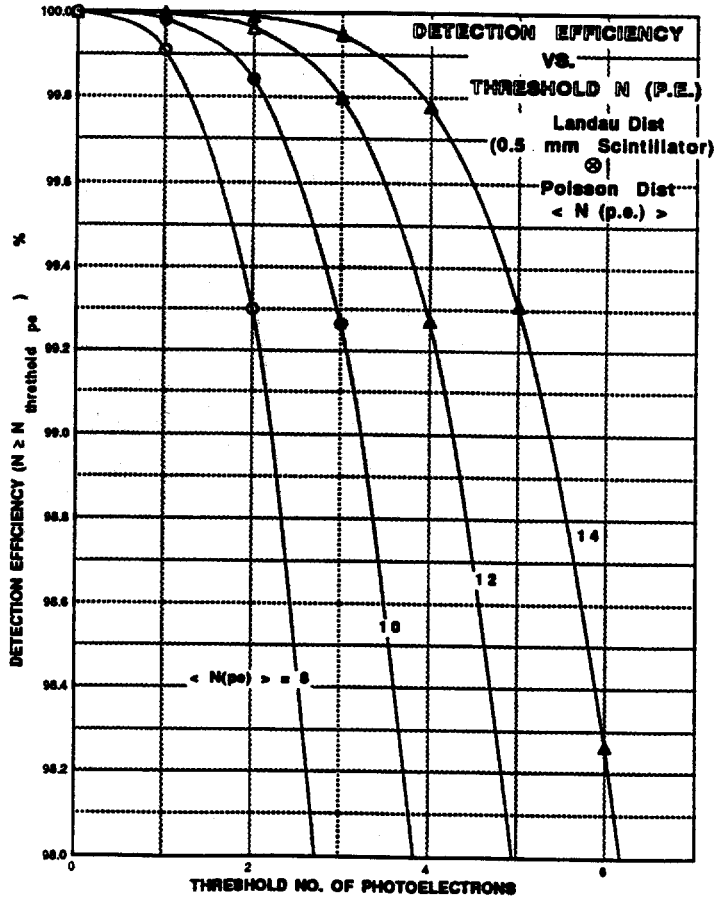
DETECTION EFFICIENCY
VS.
THRESHOLD N (P.E.)
Landau Dist
(0.5 mm Scintillator)
⊗
Poisson Dist
< N (p.e.) >
14
12
10
< N(pe) > = 8
DETECTION EFFICIENCY (N ≥ N threshold pe) %
THRESHOLD NO. OF PHOTOELECTRONS

Fig. 27

GROOVED TRAY

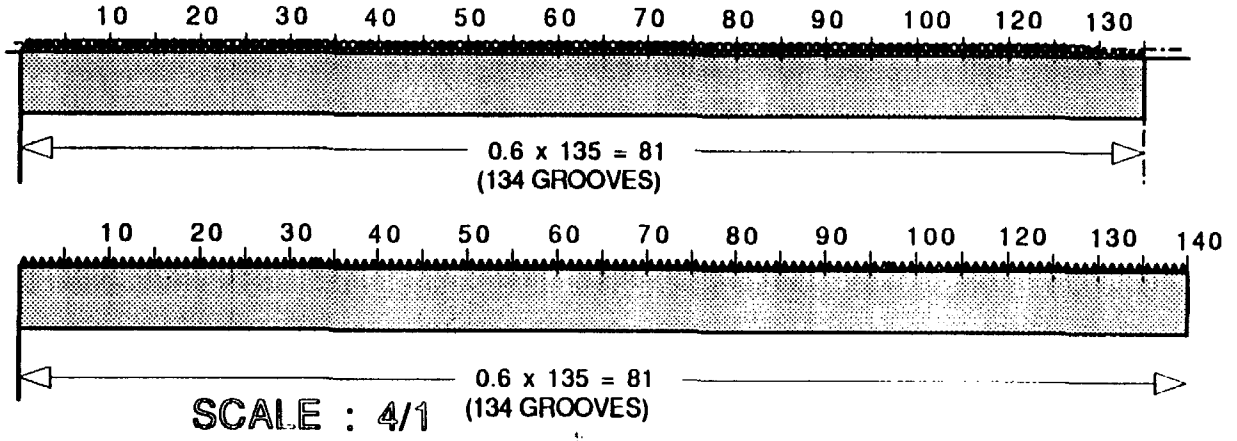

SCALE : 4/1

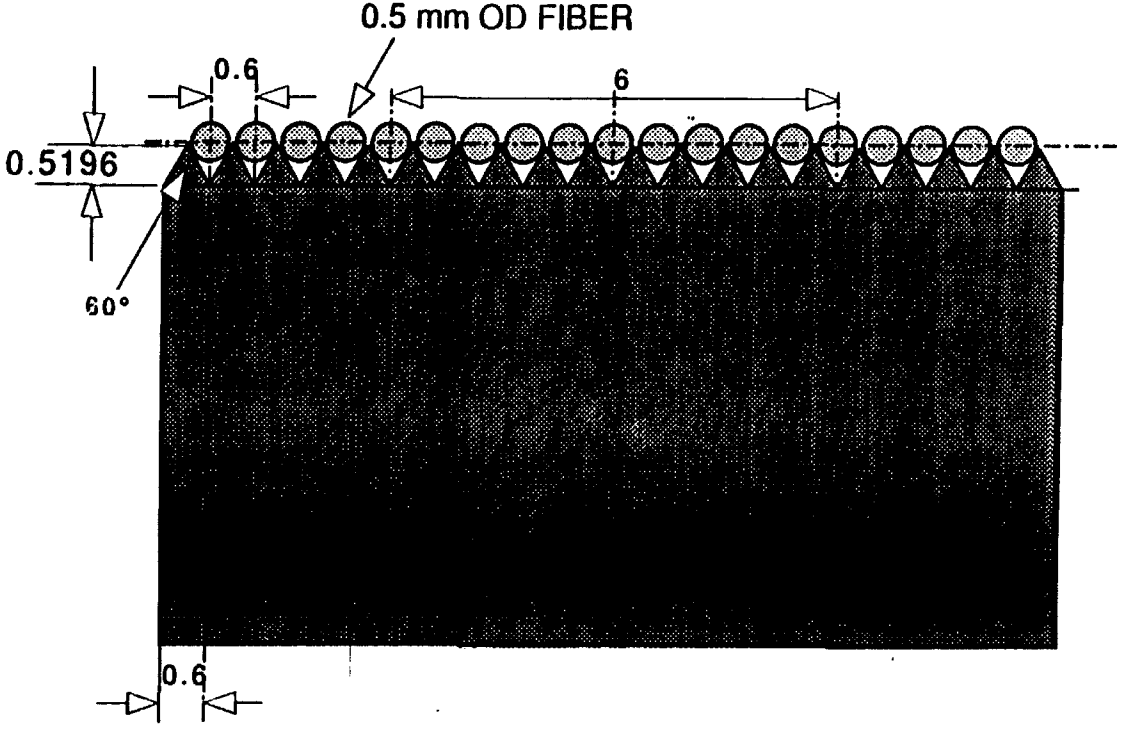

SCALE : 20/1

UNIT : mm

Fig 28

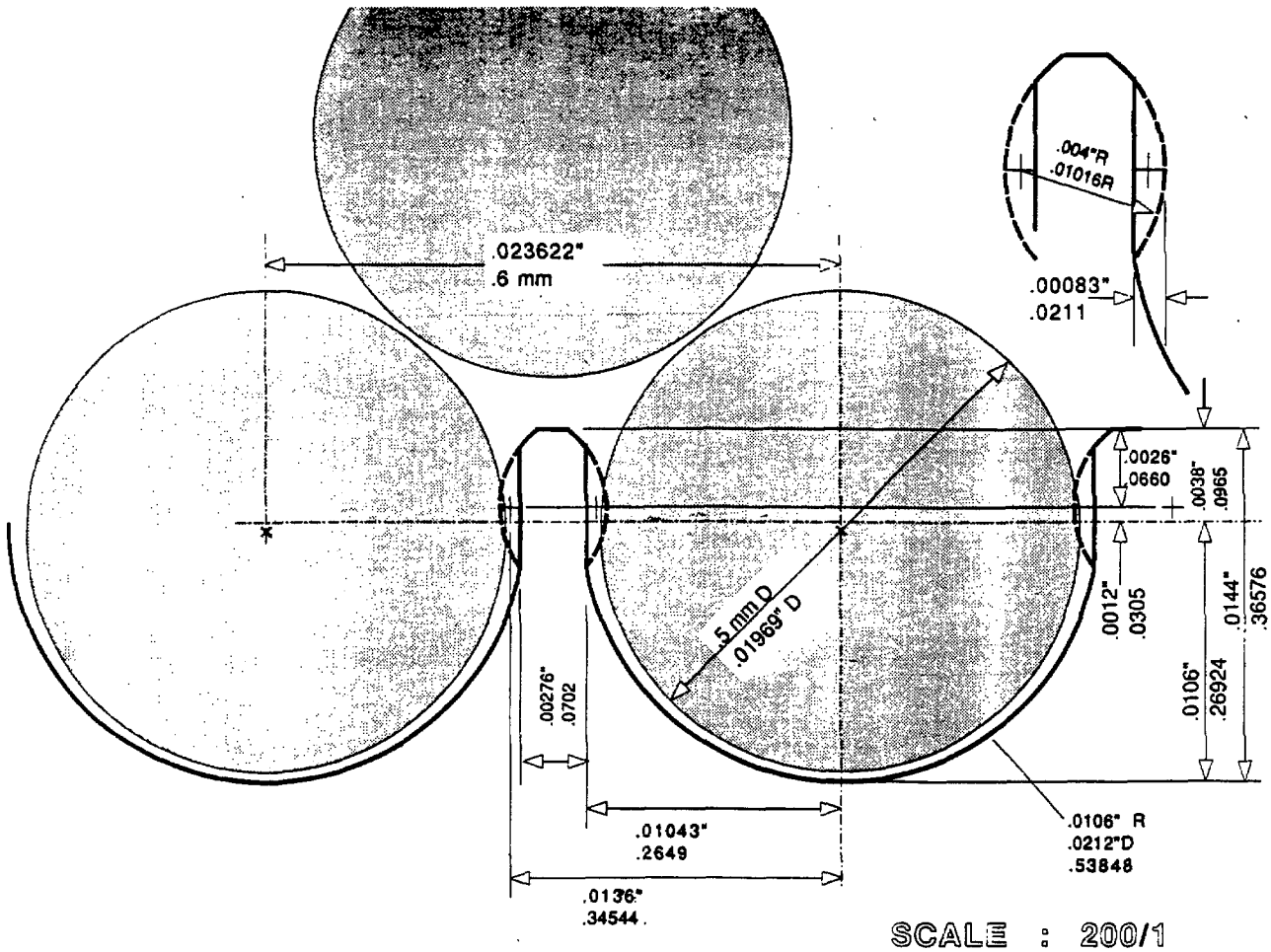
.004"R
.01016R
.023622"
.6 mm
.00083"
.0211
.0026"
.0660
.0038"
.0965
.0012"
.0305
.0144"
.36576
.0106"
.26924
.5 mm D
.01969" D
.00276"
.0702
.01043"
.2649
.0106" R
.0212"D
.53848
.0136"
.34544
SCALE : 200/1

Fig. 29

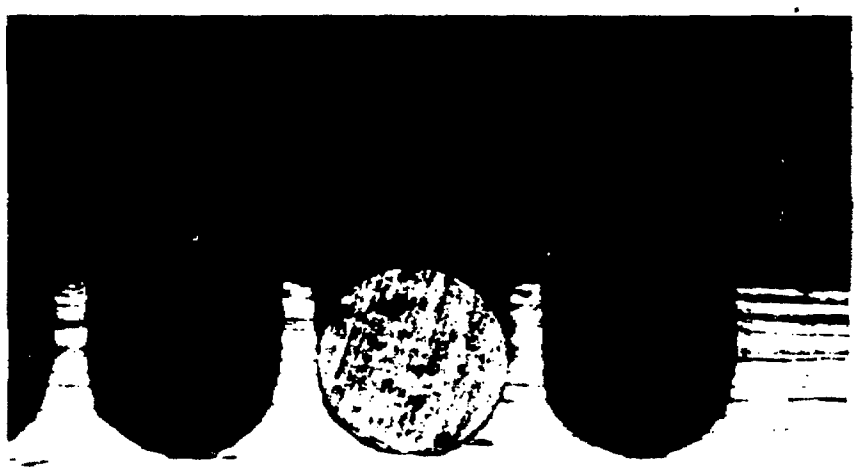

Fig. 30